



EVALUATION OF ANTIOXIDATIVE, ANTIMICROBIAL AND CYTOTOXIC ACTIVITY OF THE SYNTHETIZED ARYLMETHYLENBIS(3-HYDROXY-5,5-DIMETHYL-2-CYCLOHEXEN-1-ONE) DERIVATIVES

A. Džambić,^{[a]*} S. Muratović,^[b] E. Veljović,^[b] A. Softić,^[a] E. Dautović,^[a] M. Šljivić Husejnović,^[a] E. Horozić,^[c] A. Smajlović^[a]

Keywords: Tetraketones; cyclohexen-1-one derivatives; synthesis; antioxidants; antimicrobial screening; cytotoxic activity.

Arylmethylenebis(3-hydroxy-5,5-dimethyl-2-cyclohexen-1-one) derivatives (aryl=2-hydroxynaphthyl (**1**) and 3,4-dihydroxyphenyl (**2**)) have been synthesized and their structures have been elucidated. Both compounds were examined for their antioxidant, antimicrobial and cytotoxic activity. Antioxidative activities of synthesized compounds were evaluated by 2,2-diphenyl-1-picryl-hydrazyl (DPPH) and ferric reducing antioxidant power (FRAP) methods. The microbial screening was performed by diffusion method on bacterial strains *Staphylococcus aureus*, *Enterococcus faecalis*, *Bacillus subtilis* and *Candida albicans*. Cytotoxic activity was tested on liver hepatocellular carcinoma cell line (Hep G2) by Neutral red assay. Compared to compound **2**, compound **1** showed better antimicrobial and antifungal activity, while compound **2** showed better antioxidant activity with IC₅₀ of 0.0156 mM and FRAP value 50469.44 μmol/l Fe²⁺. Both compounds showed cytotoxic activity. Obtained results implicate the importance of arylmethylenebis(3-hydroxy-5,5-dimethyl-2-cyclohexen-1-on) derivatives as a potential antioxidant, antimicrobial and cytotoxic agents.

* Corresponding Authors

E-Mail: amra.hadziibrisevic@untz.ba

- [a] Faculty of Pharmacy, University of Tuzla, Urfeta Vejzagića 8, 75 000 Tuzla, Bosnia and Herzegovina
 [b] Faculty of Pharmacy, University of Sarajevo, Zmaja od Bosne 8, 71 000 Sarajevo, Bosnia and Herzegovina
 [c] Faculty of Technology, University of Tuzla, Urfeta Vejzagića 8, 75 000 Tuzla, Bosnia and Herzegovina

there is a real need for the development of new effective and antibacterial agents. Recent studies of tetraketones show that different such derivatives show antibacterial as well as antiviral activity.¹⁹

Previous studies of some xanthenes indicate that xanthenes have shown cytotoxic activity against human Colo-205.²⁰ Another study confirmed the antiproliferative activity of xanten-3-one derivatives against different human cell lines including SW620, HepG2, HeLa and A549 tumor cells.²¹ Thioxanthenes and xanthendiones are formed as products of cyclization of tetraketone by nucleophilic addition of hydroxyl group -OH to the C=C bond,^{22,23} therefore, their biological activity may be related to the formation of these compounds.²⁴

The aim of this study was to synthesize two new biologically active tetraketones via Knoevenagel condensation and Michael addition of benzaldehydes with dimedone and catalyst, and to evaluate their antioxidative and antimicrobial activities, as well as to assess their cytotoxic effect on human liver hepatocellular carcinoma cell line (HepG2).

INTRODUCTION

Arylmethylenebis(3-hydroxy-5,5-dimethyl-2-cyclohexen-1-one) derivatives, generally known as tetraketones, are used as important precursors for organic synthesis of heterocyclic compounds,¹ such as acridindiones, thioxanthenes,² and xanthenes.³ These compounds have a wide range of biological activities.⁴ They have strong antioxidative potential⁵ and significant inhibitory effects on enzyme activities such as lipooxygenase,⁶ tyrosinase^{7,8} and protein kinase activity.⁹ Lately, derivatives of tetraketones, due to their strong antioxidative activity,¹⁰ have received great attention as therapeutically efficient agents against disorders in which oxidative stress plays a significant role, such as inflammation,¹¹ asthma¹² and cancer.¹³

Antioxidants compounds act to stop or inhibit the oxidation process, in low concentrations, by getting themselves oxidized.¹⁴ Therefore, there has been an increased interest for the use of antioxidants in medical treatments due to their capacity to prevent oxidative stress-induced damage.¹⁵ Synthetic antioxidants such as, butylated hydroxyanisole (BHA) and butylated hydroxytoluene (BHT), most commonly used in the food industry, show significant side effects. Consequently, development of new, safe and more effective antioxidants is of major interest for the pharmaceutical and food industry.¹⁶

Antibiotics, as products of secondary metabolites of microorganisms and fungi¹⁷, are compounds used to kill or inhibit the growth of bacteria.¹⁸ Frequent and uncontrolled use of antibiotics results in resistance in bacterial strains, so

EXPERIMENTAL

The chemicals used in the synthesis of arylmethylenebis(3-hydroxy-5,5-dimethyl-2-cyclohexen-1-one) derivatives were obtained from the Merck (Darmstadt, Germany) and Sigma Aldrich (Missouri, SAD). All analyses were performed using analytical grade chemicals, reagents and standards. Neutral red assay kit was obtained from Sigma Aldrich (Missouri, SAD). For all dilutions, only double-distilled deionized water was used. □

Melting points of compounds were determined by capillary method on Kruss Melting point KSP I. IR spectra of synthesized compounds were recorded by Thermo Scientific Nicolet iS10 FTIR Spectrophotometer. The ¹H

and ¹³C nuclear magnetic resonance (NMR) spectra were recorded at 500 and 150 MHz in deuterated acetone at 25 °C using NMR spectrophotometer Bruker Avance III 500 (500 MHz for ¹H, 125 MHz for ¹³C). Elemental microanalyses of synthesized compounds were performed by ELEMENTAR (C, H, N, S, O) VARIO EL III. Antioxidant activities were recorded by Spectrophotometer UVmini-1240, Shimadzu Corporation.

General procedure for the synthesis

A mixture of 5,5-dimethylcyclohexyne-1,3-dione (2 mM), substituted benzaldehyde (1 mM) and DABCO (10 mM) in water (20 mL) was refluxed for 30 min. After completion of the reaction, the mixture was cooled to the room temperature. The solid was filtered off, washed with distilled water and recrystallized from 96 % ethanol.

Determination of antioxidant activity

2,2-Diphenyl-1-picryl-hydrazyl (DPPH) method was performed as described earlier by Lee *et al.*²⁵ The radical scavenging effect (%) or percent inhibition of DPPH radical was calculated according to the equation:

$$\% \text{ inhibition} = (A_{\text{control}} - A_{\text{sample}}) / A_{\text{control}} \times 100$$

where A_{sample} is the absorbance of the solution containing the sample at 517 nm and A_{control} is the absorbance of the DPPH solution. The results are expressed as the IC_{50} value (mM) or the concentration of the sample that caused 50 % neutralization of DPPH radicals.

The determination of ferric reducing antioxidant power or ferric reducing ability (FRAP assay) was performed by the method of Jiménez-Aspee *et al.*²⁶ To prepare the calibration curve, solutions of FeSO₄·7H₂O were prepared in the concentration range from 200 to 1000 μmol L⁻¹ ($y = 0.001x + 0.0615$; $R^2 = 0.9907$). In each tube, 0.1 mL of sample and 3 mL of FRAP reagent were added. The samples were incubated in an aqueous bath for 30 min at 37 °C, and the absorbance was measured at 593 nm.

Determination of antimicrobial activity

Antimicrobial activity was determined using the diffusion the method described by Pirvu *et al.*²⁷ on reference bacterial strains from Gram-positive microorganisms (*Staphylococcus aureus* ATCC 25923, *Enterococcus faecalis* ATCC 51299, *Bacillus subtilis* ATCC 23857). Antifungal activity was examined on *Candida albicans* (ATCC 90028). From the bacterial strains of overnight cultures, suspensions of 0.5 McFarland turbidity were prepared (density 10⁷-10⁸ CFU mL⁻¹, depending on soy). The strains were placed then on the surface of the nutrient substrate-Mueller-Hinton agar (MH), dispersed in sterile Petri dishes. The substrate thickness was 4 mm. In the agar, sterile drill-shaped holes were made ("wells"), into which 50 μL of synthesized compounds (1-2) in concentration of 2 mg mL⁻¹ were added. After the plates were left at room temperature for 15 min to the substance was diffused into agar, they were incubated at 37 °C for 24 h. After the incubation period, the size of the

inhibitory zone was measured and the sensitivity of the microorganisms was expressed as follows. If the zone for inhibition of microorganism growth was greater than 20 mm, it was labeled with three pluses (+++), representing the highest sensitivity of the microorganisms. If the inhibitory zone ranged from 16 to 20 mm, it was marked with two pluses (++) . If the inhibitory zone was 10-15 mm in diameter, it was marked with a plus (+). For the inhibitory zone, less than 10 mm or if absent, a minus (-) sign has been used.

In vitro determination of cytotoxic activity

The liver hepatocellular carcinoma cell line was cultured in Minimum Essential Medium Eagle medium (Sigma Aldrich) containing 2 mM glutamine (Sigma Aldrich), 1 % nonessential Amino Acids (Sigma Aldrich), 10 % heat-inactivated (HI) FBS (Sigma Aldrich) and 1 % penicillin/streptomycin antibiotics (Sigma Aldrich), in a humidified atmosphere containing 5 % CO₂ at 37 °C. For each experiment, cells were grown at 80 % confluence in 75 cm² culture flasks.

Cytotoxic activity (cell viability) was evaluated by Neutral red assay using the method previously described by Repetto *et al.*²⁸ For each experiment, HepG2 cells were seeded (2 x 10⁴ cells well⁻¹) in 96 well plates and grown for 24 h. Test agents (2.5 μM-100 μM) were then added and cells were incubated for an additional 24 h. Working dilutions were freshly prepared on the day of testing in the growth medium. The solvent (DMSO) concentration never exceeded 0.1 % in the final medium containing cells. Untreated cells were used as negative control and positive control were cells treated with 5-fluorouracil (5-FU). Cells were treated with 10 % compound solutions and 90 % culture medium. Compound stock solutions were prepared in double-distilled deionized water and solutions were sterilized by filtration through 0.2 μm sterile syringe filters.

The Neutral red assay was carried out according to the manufacturer's instructions (Sigma Aldrich). After 24 h treatment cells were incubated with medium containing neutral red dye for 3 h. The cells were subsequently washed, the dye was extracted from cells and absorbance was measured using a microplate reader at a wavelength of 540 nm. The measured absorbance values were converted to percent of cell viability with respect to negative control. □

RESULTS AND DISCUSSION

Synthesis of arylmethylenebis(3-hydroxy-5,5-dimethyl-2-cyclohexen-1-one) derivatives

As shown in Figure 1, the synthesis of arylmethylenebis 3-hydroxy-5,5-dimethyl-2-cyclohexen-1-ones was assumed to proceed via forming a product of Knoevenagel condensation and Michael addition. In the first step of the synthesis, there is a condensation of 5,5-dimethylcyclohexane-1,3-dione and the 2-naphthylaldehyde and 3,4-dihydroxyphenylaldehyde. After dehydration and Michael's addition, synthesized tetraketone converts to aryl methylenebis(3-hydroxy-5,5-dimethyl-2-cyclohexen-1-one) derivative via keto-enol tautomerism.^{3,22}

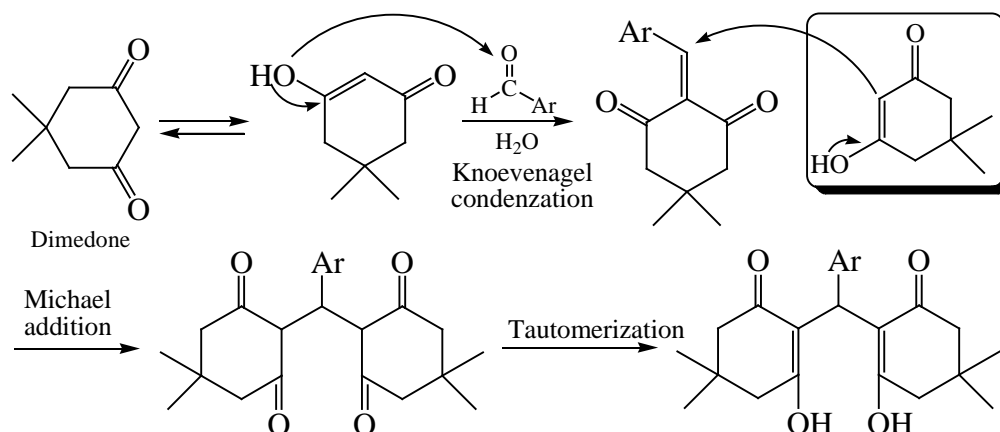


Figure 1. Mechanism of synthesis of 2,2'-arylmethylen-bis(3-hydroxy-5,5-dimethyl-2-cyclohexen-1-one) derivatives.

2,2'-(2-Hydroxynaphtyl)methylenebis(3-hydroxy-5,5-dimethyl-2-cyclohexen-1-one) (1)

Yield 98.80 %, m.p. 236-240 °C. IR: 3200 (O-H), 3000 (Ar-H), 2934 (Aliph. -CH), 1641 (C=O), 1590 and 1465 (C=C), 1369 (C-O), 1230(-OH) cm⁻¹. ¹H NMR (500 MHz): δ = 0.52-0.80 (4s 12H, C(CH₃)₂); 1.70-2.10 (dd, 4H, CH₂); 2.02-2.26 (dd, 4H CH₂); 5.46 (s 1H CH); 7.19-8.02 (6 d, 6H, Ar-H); 11.09 (s, 1H, -OH). ¹³C NMR δ = 26.5-30.0 (CH₃ on C₅ and C_{5'}); 30.07 (C₅ and C_{5'}); 32.2 (C₇); 41.6, 43.7 (C₄ and C_{4'}); 50.3, 51.3 (C₆ and C_{6'}); 111.9 (C₂ and C_{2'}); 117.4, 132.2, 149.9 (Ar-C); 117.5, 123.9, 125.2, 127.4, 129.2, 120.4 (Ar-CH); 195.5, 200.9 (C₁ and C_{1'}); Anal. Calcd for C₂₇H₃₀O₅: C 74.63, H 6.96. Found C 74.98, H 6.59.

2,2'-(3,4-dihydroxyphenyl)methylenebis(3-hydroxy-5,5-dimethyl-2-cyclohexen-1-one) (2)

Yield 53.50 %, m.p. 196.5-198.5 °C. IR: 3236 (O-H), 3000 (Ar-H), 2966 (Aliph CH), 1652 (C=O), 1558 and 1467 (C=C), 1369 (C-O), 1249 (OH) cm⁻¹. ¹H NMR: δ = 1.14 (s, 12H, C(CH₃)₂); 2.12 (s, 4H, CH₂); 2.38 (s, 4H CH₂); 5.41 (s, 1H, CH); 6.64; 6.69 (dd, 3H Ar-H); 7.67; 7.69 (s, 2H, OH); 12.01 (s, 1H, OH). ¹³C NMR: δ = 28.6 (CH₃ on C₅ and C_{5'}); 32.2 (C₅ and C_{5'}); 33.0 (C₇); 47.3 (C₄, C₆ and C₄, C₆); 115.5, 115.9, 119.2, 131.0 (Ar-CH) 144.0, 145.8 (Ar-C); 116.5 (C₂ and C_{2'}); 190.4 (C₁, C₃ and C₁, C₃). Anal. Calcd for C₂₃H₂₈O₆: C 68.98, H 7.05. found C 68.77, H 6.82.

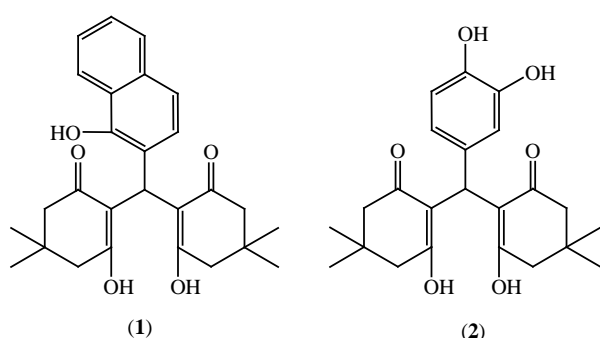


Figure 2. Structure of synthesized compounds, 1 and 2

Structural characterization of compounds

The IR spectrum indicated that both samples show absorption bands for tetraketone structure, stretching vibrations between 3000-2900 cm⁻¹ came from aliphatic CH group, absorption bands at 1700-1600 cm⁻¹ belong to C=O groups. Further, all IR spectrum show bands at 1600 and 1446 cm⁻¹ which are characteristic for the aromatic ring (C=C), there are bands at 1300 cm⁻¹, characteristic for C-O stretching and deformation vibrations of the OH group at 1200 cm⁻¹. The aromatic hydroxy groups as substituents in the spectrum of compound 1 with 2-hydroxynaphtyl group show a characteristic band at 3200 cm⁻¹, while the spectrum of compound 2 with two hydroxy groups on phenyl ring on the positions of 3 and 4, has a characteristic band at 3236 cm⁻¹.

The ¹H NMR spectra of synthesized compounds contain broad singlets in the range of 1.14-1.18 ppm derived from CH₃ protons belong to positions C₅ and C_{5'}. Both spectra have 2-2 singlets in the range of 2.03-2.12 ppm and 2.38-2.41 ppm due to CH₂ protons on positions of C₄, C₆, and C₄, C₆. One singlet was observed at 5.41-5.46 ppm from CH proton, which connects cyclohexene rings (C₇).

A singlet at 4.29 ppm (proton of the hydroxy group) and three doublets in the range of 7.19-7.36 ppm and doublets in the range of 7.26-8.02 derived from the protons of the naphthyl group could be observed in the spectrum of compound 1. Two doublets were found at 6.64-7.52 ppm due to phenyl ring protons of compound 2, while the hydroxy group signals had a singlet at 6.97-7.67 ppm

The ¹³C NMR spectra of synthesized compounds showed signals at 26.5-29.0 ppm belong to carbon atoms of the methyl groups. The signals from carbons on positions C₅ and C_{5'} are at 30.07-32.8 ppm, while the signal from the methine group connects the two cyclohexene rings that appeared at 32.2-33.6 ppm. Signals characteristic for cyclohexene ring appeared at 47.6-51.3 (C₄, C₆ and C₄, C₆), 111.9-116.6 (C₂ and C_{2'}) and 190.4-200.9 ppm (C₁, C₃ and C₁, C₃). In the ¹³C NMR spectra, signals for aromatic carbons appeared at 117.4-125.2 and 127.4-132.2 ppm or 112.2-129.0 and 131.0-150 ppm for compound 1 and compound 2, respectively.

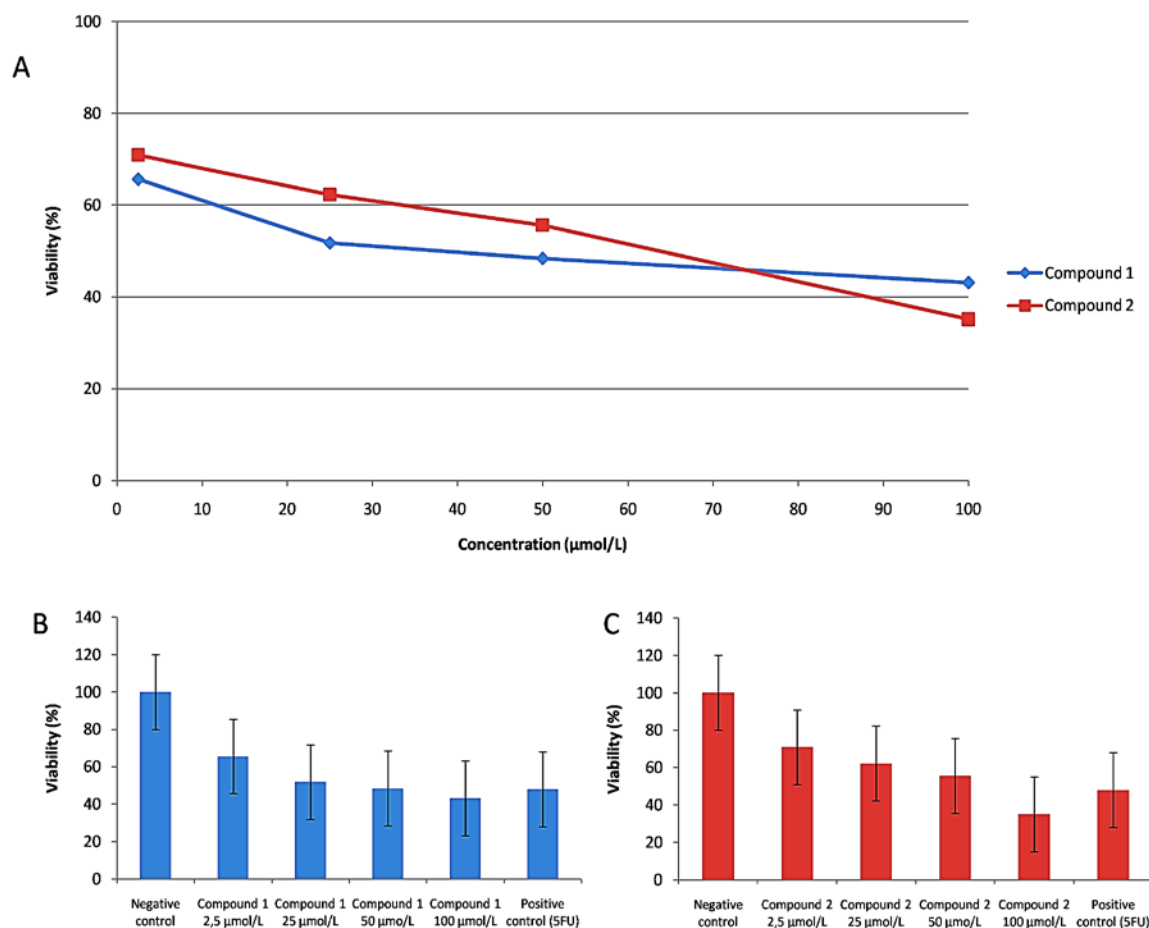


Figure 3. A. Viability of HepG2 cells after 24 hours exposure to increasing concentrations (2.5 µM, 25 µM, 50 µM and 100 µM) of compound 1 and compound 2. B. Effects of compound 1 on cell viability in the treated, negative control, and positive control HepG2 cells. Mean ± SD of triplicates in a representative experiment. C. Effects of compound 1 on cell viability in the treated, negative control, and positive control HepG2 cells. Mean ± SD of triplicates in a representative experiment.

Antioxidant activity

The results of antioxidant activity expressed as IC_{50} and FRAP value, are shown in Table 1. Results indicated 2 has the strongest free radical scavenging effect with IC_{50} of 0.0156 mM and a FRAP value 50469.44 µmol L⁻¹ Fe²⁺, which may be due to the formation radical on the hydroxy group (substituted on phenyl ring in positions 3 and 4). Compound 1, substituted with two hydroxynaphthyl groups, has a free radical scavenging effect and IC_{50} of 1.79 mM and FRAP value of 290.95 µmol L⁻¹ Fe²⁺.

Table 1. Summarized results of antioxidant capacity.

Sample	IC_{50} value,	FRAP value, µmol L ⁻¹ Fe ²⁺
1	1.790	290.95
2	0.015	50469.44
Vitamin C	0.035	14250

In comparison with Vitamin C, compound 2 exhibited higher antioxidant capacity. These results suggest that hydroxy groups have a significant effect on the antioxidant activities of synthetic antioxidant substances. It has been previously reported that reducing power is associated with antioxidant activity, which is in accordance with our

findings.³⁰ Further, significant effects of hydroxy group position on antioxidative activity have been previously reported.³ Also, a good antioxidant activity of other tetraketones in the literature has been reported, which correlates with our results.³¹

Antimicrobial activity

Results of the in vitro antimicrobial activity of the synthesized compounds against selected test microorganisms are shown in Table 2. Results indicate that compound 1 has antibacterial activity against all tested Gram-positive bacteria, and has antifungal activity against *Candida albicans*. The largest inhibition zone, for compound 1, was recorded with *Staphylococcus aureus* (20 mm) and the smallest with *Enterococcus faecalis* (10 mm). Compound 2 has antimicrobial activity only against *Staphylococcus aureus* (11 mm). In comparison to compound 2, compound 1 showed more potent antimicrobial and antifungal activity. This probably occurs due to the presence of 2-naphthol group in the structure of compound 1. According to the literature the naphthalene ring, as a potent lipophilic part of the structure,³² better passes through biomembranes and therefore acts as a potent antimicrobial agent.³³

Table 2. Antimicrobial activity of compounds in diameters, in mm, of inhibition zone.

Sample	SA	EF	BS	CA
Compound 1	20 (++)	10 (+)	13 (+)	14 (+)
Compound 2	11 (+)	-	-	-
Ciprofloxacin	>25 (+++)	>25 (+++)	>25 (+++)	-
Nystatin	-	-	-	20 (++)

Legend: SA - *S. aureus*, EF - *E. faecalis*, BS - *B. subtilis*, CA - *Candida albicans*.

Cytotoxic activity

Assessment of the cytotoxic potential of tetraketones on human-derived carcinoma cell line is the subject of many scientific studies.³⁴ Our findings suggest that both of our samples are potent cytotoxic agents (Figure 3). As expected, compound **1** exhibited higher cytotoxic potential, causing a higher percent of cytotoxicity at the same concentration compared to compound **2**. It was interesting that the most pronounced cytotoxic effect was observed at the highest concentrations of compound **2** (100 $\mu\text{mol L}^{-1}$). It is noticeable that the increase in concentrations necessarily leads to a proportional decline in cell viability in both cases, respectively. These results are in agreement with previously reported data which suggest that concentrations of cytotoxic substance are in direct relationship with cell viability.²¹

CONCLUSION

Two arylmethylenebis(3-hydroxy-5,5-dimethyl-2-cyclohexen-1-one) (aryl = 2-hydroxynaphthyl (**1**) and 3,4-dihydroxy-phenyl (**2**) derivatives were synthesised and tested for antioxidant, antimicrobial and cytotoxic activities. From the results, we can conclude that better antioxidant activity with IC_{50} of 0.0156 mM and FRAP value 50 469.44 $\mu\text{mol L}^{-1}$ Fe²⁺ has been found for compound **2**, while better antimicrobial and antifungal activity could be found for compound **1**. Although both compounds showed cytotoxic activity, compound **1** exhibited higher cytotoxic potential in comparison to compound **2**. The results obtained showed significant antioxidative, antimicrobial, and cytotoxic activities which support the importance of these compounds as candidates for therapeutically efficient agents against oxidative stress, microorganisms, and tumor cells.

Acknowledgments

This work was supported by the Federal Ministry of Education and Science, Bosnia and Hercegovina, under the grant 05-39-2514-1/18 from 12th November 2018. □

REFERENCES

¹Khurana, J. M., Vij, K., A highly efficient catalyst for one-pot synthesis of tetraketones and biscoumarines, *J. Chem. Sci.*, **2012**, *124*(4), 907-912. <https://doi.org/10.1007/s12039-012-0275-8>

²Ferreira, M. S., Figueroa-Villar, J. D., Conformational analysis of 2,2'-arylmethylene-bis(3-hydroxy-5,5-dimethyl-2-cyclohexen-1-one) by NMR and molecular modeling, *J. Braz. Chem. Soc.*, **2014**, *25*(5), 935-946. <http://dx.doi.org/10.5935/0103-5053.20140065>

³Zukić, S., Veljović, E., Špirtović-Halilović, S., Muratović, S., Osmanović, A., Trifunović, S., Novaković I., Završnik, D., Antioxidant, antimicrobial and antiproliferative activities of synthesized 2,2,5,5-tetramethyl-9-aryl-3,4,5,6,7,9-hexahydro-1-*H*-xanthene-1,8(2*H*)-dione derivatives, *Croat. Chem. Acta*, **2018**, *91*(1), 1-9. <https://doi.org/10.5562/cca3225>

⁴Sheikhhosseini, E., Faryabi, M., Uncatalyzed synthesis of arylmethylene[bis(5,5-dimethyl-3-hydroxy-2-cyclohexene-1-ones)] in hot water by domino Knoevenagel/Michael reactions, *J. Appl. Chem. Res.*, **2016**, *10*(3), 91-98.

⁵Da Silva, M. L., Teixeira, R. R., Santos, L. A., Martins, F. T., Ramalho, T. C., Structural analysis of two tetraketones and theoretical investigation of the reactions involved in their preparation, *J. Mol. Str.*, **2018**, *1156*(15), 700-711. <https://doi.org/10.1016/j.molstruc.2017.11.105>

⁶Khan, K. M., Maharvi, G. M., Nawaz, S. A., Perveen, S., Choudhary, M. I., An alternative method for the synthesis of tetraketones and their lipoxygenase inhibiting and antioxidant properties, *Lett. Drug. Des. Discov.*, **2007**, *4*(4), 272-278. <https://doi.org/10.2174/157018007784620004>

⁷Ferreira, M. S., Pires, D. A. T., Figueroa Villar, J. D., Evaluation of tetraketones and xanthenediones as tyrosinase inhibitors or activators, *World J. Pharm. Sci.*, **2015**, *4*(4), 1705-1718.

⁸Khan, K. M., Maharvi, G. M., Khan, M. T. H., Shaikh, A. J., Perveen, S., Begum, S., Choudhary, M. I., Tetraketones: A new class of tyrosinase inhibitors, *Bioorg. Med. Chem.* **2006**, *14*(2), 344-351. <https://doi.org/10.1016/j.bmc.2005.08.029>

⁹Alchab, F., Ettouati, L., Bouaziz, Z., Bollacke, A., Delcros, JG., Gerdzen, C. G. W., Gohlke, H., Pinaud, N., Marchivie, M., Guillon, M., Fenet, B., Jose J., Le Borgne, M., Synthesis, biological evaluation and molecular modeling of substituted indeno[1,2-*b*]indoles as inhibitors of human protein kinase CK2, *Pharmaceuticals*, **2015**, *8*(2), 279-302. <https://doi.org/10.3390/ph8020279>

¹⁰Iqbal, L., Lateef, M., Ali, S., Rigaz, N., Maharvi, G. M., Ashraf, M., Afza, N., Antioxidant activities of tetraketones derived from 5,5-dimethylcyclohexane-1,3-dione, *J. Chem. Soc. Pak.*, **2007**, *29*(1), 51-54.

¹¹Nie, D., Honn, K. V., Cyclooxygenase, lipoxygenase and tumor angiogenesis. *Cell. Mol. Life. Sci.*, **2002**, *59*(5), 799-807. <https://doi.org/10.1007/s00018-002-8468-9>

¹²Sneider, I., Bucar, F., Lipoxygenase inhibitors from natural plant sources. Part 2: medicinal plants with inhibitory activity on arachidonate 12-lipoxygenase, 15-lipoxygenase and leukotriene receptor antagonists, *Phytoter. Res.*, **2005**, *19*(4), 263-272. <https://doi.org/10.1002/ptr.1604>

¹³Nikam, S. S., Kornberg, B. E., AMPA receptor antagonists, *Curr. Med. Chem.*, **2001**, *8*(2), 155-170. <https://doi.org/10.2174/0929867013373877>

¹⁴Vaya, J., Aviram, M., Nutritional antioxidants: Mechanism of action, analyses of activities and medical applications, *Curr. Med. Chem. - Imm., Endoc. & Metab. Agents*, **2001**, *1*(1), 99-117. <https://doi.org/10.2174/1568013013359168>

¹⁵Yildirm, A., Oktay, M., Bilaloglu, V., The antioxidant activity of leaves of *Cydonia vulgaris*, *Turk. J. Med. Sci.*, **2001**, *31*, 23-27.

¹⁶Fukushima, I. N., Hasegawa, S., Shibata, A., Ogiso, T., Carcinogenicity of butylated hydroxyanisole in F344 rats, *J. Natl. Cancer. Int.*, **1983**, *70*, 343-347.

¹⁷Bentley, R., Bennett, J. W., What Is an Antibiotic? Revisited, *Adv. Appl. Microbiol.*, **2003**, *52*, 303-331. [https://doi.org/10.1016/S0065-2164\(03\)01012-8](https://doi.org/10.1016/S0065-2164(03)01012-8)

- ¹⁸Van Elsas, J. D., Bailey, M. J., The ecology of transfer of mobile genetic elements, *FEMS Microbiol. Ecol.*, **2002**, 42(2), 187-197. <https://doi.org/10.1111/j.1574-6941.2002.tb01008.x>
- ¹⁹Ferreira, M. S., FigueroaVillar, J. D., Conformational Analysis of 2,2'-arylmethylene bis(3-hydroxy-5,5-dimethyl-2-cyclohexene-1-one) by NMR and Molecular Modeling, *J. Braz. Chem. Soc.*, **2014**, 25(5), 935-946. <https://doi.org/10.5935/0103-5053.20140065>
- ²⁰Bhattacharya, A. K., Rana, K. C., Mujahid, M., Sehar, I., Saxena, A. K., Synthesis and in vitro study of 14-aryl-14H-dibenzo[a,j]xanthenes as cytotoxic agents. *Bioorg. Med. Chem. Lett.*, **2009**, 19(19), 5590-5593. <https://doi.org/10.1016/j.bmcl.2009.08.033>
- ²¹Veljović, E., Špiritović-Halilović, S., Muratović, S., Osmanović, A., Haverić, S., Haverić, A., Hadžić, M., Salihović, M., Malenica, M., Sapčanin, A., Završnik, D., Antiproliferative and genotoxic potential of xanthen-3-one derivatives, *Acta Pharm.*, **2019**, 69(4), 683-694. <https://doi.org/10.2478/acph-2019-0044>
- ²²Paliwal, P., Jetti, S. R., Bhatewara, A., Kadre, T., Jain, S., DABCO catalyzed synthesis of xanthen derivatives in aqueous media, *Int. Sch. Res. Notices*, **2013**. <https://doi.org/10.1155/2013/526173>
- ²³Chen, J., Shi, J., Yan, C. G., Synthesis of spiro dihydrofurans and 1,8-dioxo-xanthenes via DABCO catalyzed tandem reaction of aldehyde with cyclohexane-1,3-dione and dimedone, *Chem. Res. Chin. Univ.*, **2011**, 27(1), 49-53.
- ²⁴Lambert, R. W., Martin, J. A., Merrett, J. H., Parkes, K. E. B., Thomas, J. G., PCT Int Appl. WO 9706178 Chem Abstr **1997**, 126:212377y
- ²⁵Benvenuti, S., Pellati, F., Melegari, M., Bertelli, D., Polyphenols, Anthocyanins, Ascorbic Acid, and Radical Scavenging Activity of Rubus, Ribes, and Aronia, *J. Food Sci.*, **2004**, 69(3), 164-169. <https://doi.org/10.1111/j.1365-2621.2004.tb13352.x>
- ²⁶Jiménez-Aspee, F., Quispe, C., Soriano, C. M. P., Fuentes, Gonzalez, J., Hüneke, E., Theoduloz, C., Schmeda-Hirschmann, G., Antioxidant activity and characterization of constituents in copao fruits (*Eulychnia acida* Phil., Cactaceae) by HPLC-DAD-MS/MSⁿ, *Food Res. Int.*, **2014**, 62, 286-298. <https://doi.org/10.1016/j.foodres.2014.03.013>
- ²⁷Pirvu, L., Hlevca, C., Nicu, I., Bubueanu, C., Comparative analytical, antioxidant and antimicrobial activity studies on a series of vegetal extracts prepared from eight plant species growing in Romania, *J. Planar. Chromat.*, **2014**, 27(5), 346-356. DOI:10.1556/JPC.27.2014.5.4
- ²⁸Repetto, G., del Peso, A., Zurita, J. L., Neutral red uptake assay for the estimation of cell viability/cytotoxicity, *Nat. Protoc.*, **2008**, 3(1), 1125-1131. <https://doi.org/10.1038/nprot.2008.75>
- ²⁹Yen, G. C., Chen, H. Y., Lee, C. E., Measurement of antioxidant activity in metal ion-reduced lipid peroxidation systems, *J. Sci. Food Agric.*, **1999**, 79(9), 1213-1217.
- ³⁰Maharvi, G. M., Ali, S., Riaz, N., Afza, N., Malik, A., Ashraf, M., Iqbal, L., Lateef, M., Mild and efficient synthesis of new tetraketones as lipoxygenase inhibitors and antioxidants, *J. Enzyme Inhib. Med. Chem.*, **2008**, 23(1), 62-66. <https://doi.org/10.1080/14756360701408754>
- ³¹Azam, F., Singh, S., Kohokhra, S. L., Prakash, O., Synthesis of Schiff bases of naphtha[1,2-d]thiazol-2-amine and metal complexes of 2-(2'hydroxy)benzylideneaminonaphthothiazole as potential antimicrobial agents, *J. Zhejiang Univ. Sci. B.*, **2007**, 8(6), 446-452. <https://doi.org/10.1631/jzus.2007.B0446>
- ³²Rokade, Y. B., Sayyed, R. Z., Naphthalene derivatives: A new range of antimicrobials with high therapeutic value, *Rasayan J. Chem.*, **2009**, 2(4), 972-980.
- ³³Mohareb, R. M., Al Farouk, F. O., Wardakhan, W. W., Uses of dimedone for the synthesis of new heterocyclic derivatives with anti-tumor, c-Met, tyrosine, and Pim-1 kinases inhibitions, *Med. Chem. Res.*, **2018**, 27(8), 1984-2003. <https://doi.org/10.1007/s00044-018-2208-7>

Received: 17.05.2020.

Accepted: 08.06.2020



STUDY OF AEROSOL OPTICAL DEPTH CLIMATOLOGY USING MODIS REMOTE SENSING DATA

Amaury de Souza,^{[a]*} Marcel Carvalho Abreu,^[b] José Francisco de Oliveira-Júnior,^[c] Cícero Manoel dos Santos,^[d] Ivana Pobocikova,^[e] Widinei A. Fernandes,^[a] Emmanuel Torsen,^[f] Elania Barros da Silva^[g] and Yohana Vandi Mbaga^[h]

Keywords: Aerosol, satellite, remote sensing, AERONET, MODIS, wildfires.

The temporal variations of the aerosols and their relations with the meteorological conditions in the center of Brazil were studied to understand their interactions with meteorological parameters. Dissimilar cyclical variations are observed due to the trends of the annual cycle: first decreasing and then increasing. Principal component analysis (PCA) may imply the reasons for different characteristics of the temporal variations of the Aerosol Optical Thickness (AOT) and also confirm that their distributions are influenced by complex interactions between different meteorological factors. The average AOT during the selected period has been positively correlated with the thermal and pollutant variables, but negatively correlated with the humid variables.

* Corresponding Authors

- E-Mail: amaury.de@uol.com.br
- [a] Federal University of Mato Grosso do Sul, C.P. 549, 79070-900. Campo Grande, MS, Brazil
- [b] Universidade Federal Rural do Rio de Janeiro, Seropédica, Rio de Janeiro, Brasil
- [c] Universidade Federal de Alagoas, Instituto de Ciências Atmosféricas (ICAT), Maceió, Brazil
- [d] Federal University of Para, Altamira, PA, Brazil
- [e] Department of Applied Mathematics, Faculty of Mechanical Engineering, University of Zilina, Slovakia
- [f] Department of Statistics and Operations Research, School of Physical Sciences, Modibbo Adama University of Technology Yola, Nigeria
- [g] Secretaria Municipal de Capela (SMC), Capela, 57780-000, Alagoas, Brasil
- [h] Department of Statistics and Operations Research, School of Physical Sciences, Modibbo Adama University of Technology Yola, Nigeria

satellite remote sensing and terrestrial observations have become widely used to monitor spatial and temporal distributions of aerosols at both global and local scale.¹⁵⁻¹⁷ Satellite instruments such as Moderate Resolution Imaging Spectroradiometer (MODIS) are used to monitor regional and global scale aerosols and provide continuous and long-term coverage of the territory under study.

Aerosols are closely related to a set of meteorological variables: pressure (*PRS*), average temperature (*TEM*), relative humidity (*RHU*), precipitation (*PREC*), evaporation (*EVP*), wind speed (*WSP*), wind direction (*WDI*), sunshine duration (*SSD*), and the individual effects of various weather factors on particulate matter (*PM*) concentrations. The *PM* concentrations are also very sensitive to temperature, humidity, wind speed, and precipitation.^{10,18-23}

INTRODUCTION

The atmospheric aerosol consists of solid and liquid particles suspended in the atmosphere, studies of its physical characteristics and chemical composition allow anticipating possible climate changes, with ecological and long-term consequences.^{1,2} Atmospheric aerosols resulting from the burning of biomass, dust minerals, volcanic ashes, smoke, sea salt, and particulate matters, stand out amongst the various natural and anthropogenic influences. Aerosols are important components of the Earth system³ and decisively influence global and regional climate change,^{4,5} air quality,⁶ human health,⁷⁻¹¹ the fauna, flora and the environment¹² through direct action and indirect radiation forcing, in addition to directly impacting the cloud processes¹³ and visibility variation.¹⁴ Aerosols have a significant impact on gas concentration, distribution, and the hydrologic cycle of the greenhouse effect, affecting the physical and chemical processes occurring in the atmosphere.

Aerosol optical thickness (*AOT*) is the most comprehensive variable for remote assessment of aerosol loading in the atmosphere and is used to reflect its column loading. Recently,

There are few studies on how aerosol distribution depends on the complex effects of these weather factors. In this paper, *AOT* and all major meteorological factors were investigated together with aerosol meteorology. Aerosol data of MODIS Tier 2 products has been applied to Principal Component Analysis (PCA) to evaluate statistical relationships between seasonal distributions of average *AOTs* and meteorological factors. PCA is a statistical technique used to reduce the total number of parameters to a more manageable number by grouping linearly correlated observations into a smaller number of variables in PC space.²⁴ In addition, this technique combines highly correlated observation information into new principal components (PC) variables, which are often uncorrelated with each other. Initially, the spatial distribution and temporal variation of *AOT* are evaluated for the central part of Brazil for the period from 2002 to 2011. The objective is to link the properties of aerosol distributions to regional weather conditions.

EXPERIMENTAL

The aerosol concentrations were inferred monthly from the *AOT* data at 550 nm of the MODIS/Terra sensor, whose

spatial resolution is 100 km. These data come from the NASA Giovanni database. *AOT* is a non-dimensional physical parameter and indicates how much a beam of radiation is attenuated by aerosols as it propagates in a certain layer of the atmosphere containing aerosols.

The daily records of the O_3 and CO concentration present in the atmosphere and the meteorological data during the study period were provided by the Federal University of South Mato Grosso, where the monitoring station is located. The clarity index (K_t), given by Eqn. (1), determines the sky coverage, defined as the ratio of incident solar radiation (R_g) ($MJ\ m^{-2}\ day^{-1}$) by the top of the atmosphere radiation (R_0).

$$K_t = \frac{R_g}{R_0} \quad (1)$$

The lightness index (K_t) was determined by the sky cover according to Souza *et al.*,¹⁰ according to which the global and diffuse radiations are practically the same in the interval $0 < K_t < 0.3$, and the radiation of direct approach is close to zero, classifying the sky under these conditions as cloudy. For the interval $0.3 < K_t < 0.65$, the diffuse and direct radiations remain close, denominating the sky as partly cloudy. When the interval is comprised of between $0.65 < K_t < 1$, the direct approaches the global radiation, while the diffuse radiation tends to have minimum value. In these conditions the sky is called clean.

For numerical purposes, aerosols dependent variables are called Y , and the independent variables are X , for the considered period of study. The transformation of the year variable into the year-centered variable – year minus the midpoint of the studied period – becomes necessary, since in polynomial regression models, the terms of the equation are often highly correlated and express the independent variable. Deviation from their mean value is substantially reduced to the self-correlation among them. A trend analysis of the historical series was performed using a multiple linear regression model that best described the relationship between the independent variable X , i.e., the ozone concentration, the number of heat sources, precipitation, minimum and maximum temperatures, relative humidity, velocity of winds, and the dependent variable Y , aerosol concentration, according to Eqn. (2).

$$Y = \beta_0 + \beta_1 X_1 + \beta_2 X_2 + \dots + \beta_k X_k + \varepsilon \quad (2)$$

Here the index k represents the number of variables, X_j – regressors, β_j – estimators and ε – standard error. As a measure of precision, the coefficient of determination R^2 was used. The analysis of the residues confirmed the homoscedasticity assumption of the model.^{25,26}

Statistical analysis

In this study, a descriptive analysis of the variables was performed and, later, the hypotheses were tested using the Multiple Regression Models (Eqn. 3).

The mean square error (MSE) was calculated to check the dexterity of the model.

$$MSE = \sqrt{\frac{1}{n} [\sum_{i=1}^n (P_i - O_i)^2]} \quad (3)$$

Here P_i and O_i are the estimated and the observed values respectively. The significance level of 5 % was considered in all analyses. For consideration of variables, the data standardization was used to apply the statistical technique, considering the principal component analysis (PCA) and cluster method.

Principal Component Analysis

PCA allows the reduction of multiple, highly correlated variables from multiple data sources into a small number of independent variables, each one having a unique physical interaction.²⁷ It has been used²⁴ to combine MODIS clouds and aerosols products, National Centers for Environmental Prediction (NCEP) Reanalysis and TRMM-PR pluviometry data to assess aerosol impacts in South America precipitation. PCA simulation was performed using Matlab 7.1 with the algorithm described in depth by Jones and Christopher.²⁴ The initial step in PCA is the calculation of a linear correlation matrix (R) from the normalized data set (Z). Z represents an $m \times n$ matrix, where m is the number of input variables and n is the sample size of the seasonal data sets.

In this study, $m = 13$ represents the combination of thirteen variables and $n = 365$ represents the corresponding sample size for each variable. The correlation matrix was calculated from the combined dataset of aerosols and meteorological factors, where each data represents the value corresponding to a search unit during a single station. Once the correlation matrix is calculated, the eigen values (λ) and eigen vectors are calculated using Eqn. (4).

$$E^{-1} \times R \times E = \lambda \quad (4)$$

The correlation matrix and the eigen vectors are $m \times n$ matrices, and the eigen values are one-dimensional matrices of size m . The weighting coefficients (A) are calculated from the eigen values and vectors through Eqn. (5), where λ_m is a $m \times m$ matrix in which the diagonal values are set to 1 and all other values are set to 0. The values of weighting range in magnitude from -1.0 to 1.0, where 0 indicates that there is no contribution of an input variable to the new PC variable.

$$A = E \sqrt{\lambda} \times m \quad (5)$$

Once the weights have been determined, the PC (F) variables can be derived from the raw data (Z) using eqn. (6). The solution for F produces the final solution of PC variable, given by eqn. (7).

$$Z = F \times A^T \quad (6)$$

$$F = Z \times A \times (A^T \times A)^{-1} \quad (7)$$

The magnitude of an eigen value relative to the total variance of the data set can be considered the degree of variance explained by the new variable.

A greater eigen value indicates that its information is more important in relation to the complete dataset. The PC variables were ordered in such a way that the first variable (PC1) accounts for the greater variance in the raw data, the second variable (PC2) accounts for the second largest amount of variance, and so on.^{27,28}

RESULTS

The following graphics show the results of the measured variables as a function of the time along a year for the city of Campo Grande, capital city of South Mato Grosso state, Brazil. The period considered in this paper goes from 2002 to 2011, therefore, all the values exhibited have been averaged on this time interval. A second and sometimes even a third independent variable is plotted together with the optical depth for sake of graphic comparison and visual idea of correlation among them. The variable time is shown in months, the optical depth is always represented in the right y-axes, and the other independent variable scale is exhibited in the left y-axes.

The first characteristic shows the O₃ and CO concentration concomitantly with the optical depth as a function of the time along the year. All these values are obviously positively correlated as all their characteristics follow similar shapes. The second graphic shows the temperatures – minimum, maximum and average values – also with the optical depth. The third graphic shows the humidity factor, also minimum, maximum and average values as a function of the time along the year to be compared with the optical depth. Graphic number four shows the dew point while graphic number 5 represents the atmospheric pressure, minimum, maximum and average values of both variables. Graphics number 6 and number 7 show the wind direction and wind speed respectively. Graphic number 8 exhibits the solar radiation and graphic number 9 shows the clarity index. The last two graphics, numbers 10 and 11 shows the number of wildfires spots and the precipitation level, respectively, always compared, in the same figure, with the optical depth as a function of the time along the year.

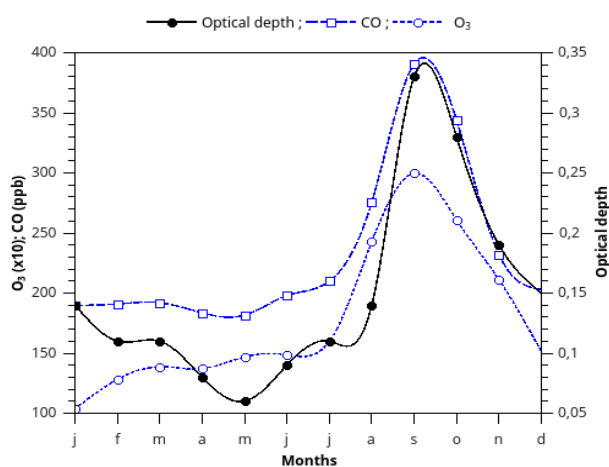


Figure 1. Measurement of ozone (O₃) – empty square – and carbon monoxide (CO) – empty circles – concentrations at left and optical depth – filled circle – at right as a function of the time along the year.

The average temperatures measured in the region are high in spring-summer, with September and October being the

hottest months (averages above 23 °C) and mild in autumn-winter, but rarely lower than 18 °C. June and July are the months with the lowest thermal averages, between 18 °C and 21 °C. The average rainfall reached by precipitation during the year present a distribution of 1330 mm.

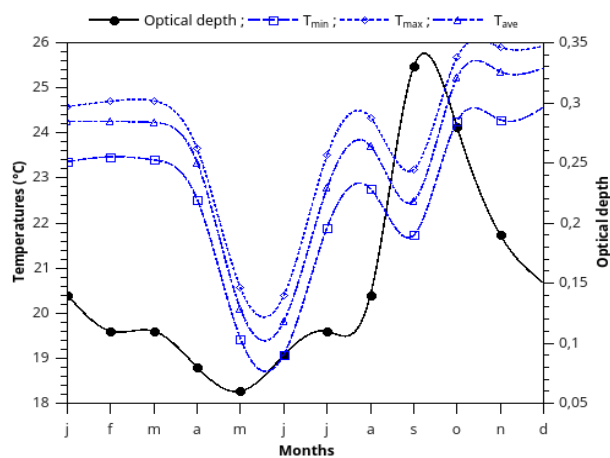


Figure 2. Measurement of the temperature – minimum, average and maximum values – at left and optical depth – filled circle – at right as a function of the time along the year.

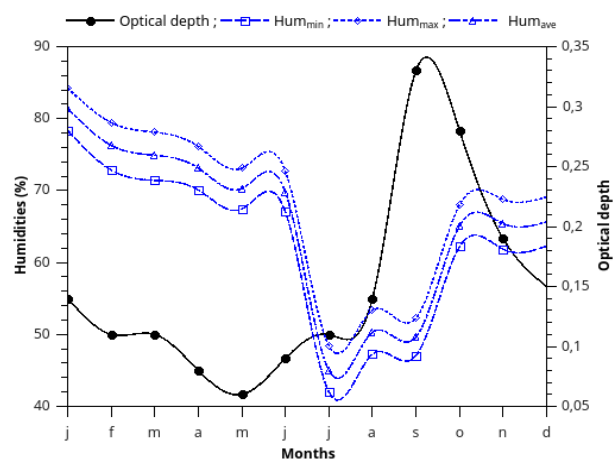


Figure 3. Measurement of the humidity – minimum, average and maximum values – at left and optical depth – filled circle – at right as a function of the time along the year.

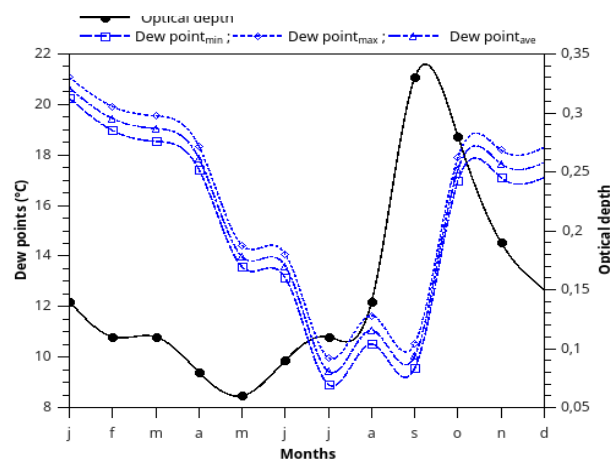


Figure 4. Measurement of the dew points – minimum, average and maximum values – at left and optical depth – filled circle – at right as a function of the time along the year.

The values of monthly and annual average recorded temperatures lead to the understanding that the spatial and seasonal variation of this climatic variable follows the characteristics of the region.

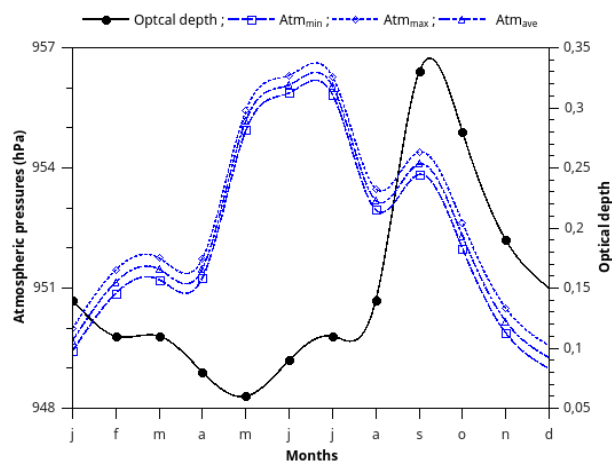


Figure 5. Measurement of the atmospheric pressure – minimum, average and maximum values – at left and optical depth – filled circle – at right as a function of the time along the year.

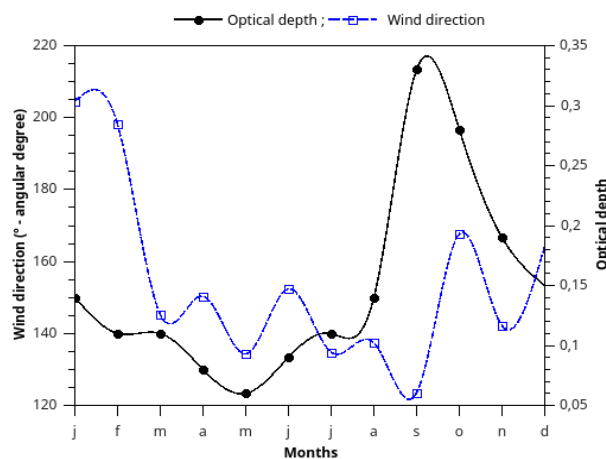


Figure 6. Measurement of the wind direction – empty square – at left and optical depth – filled circle – at right as a function of the time along the year.

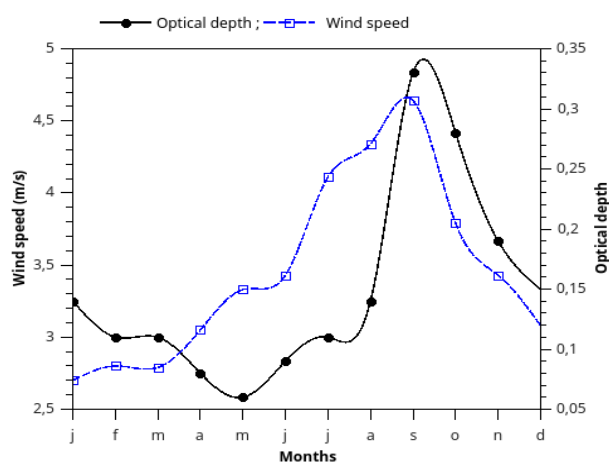


Figure 7. Measurement of the wind speed – empty square – at left and optical depth – filled circle – at right as a function of the time along the year.

The highest thermal averages are observed from October to March, which correspond to the summer in the tropical climates in the Southern Hemisphere. October is the month having the highest averages, and it is the period characterized by the transition between the dry period and rainy.

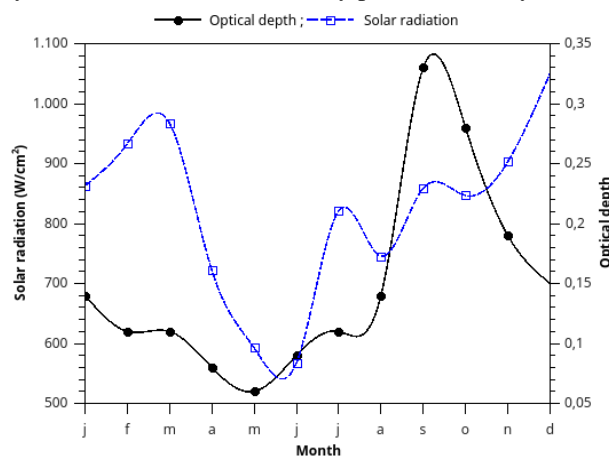


Figure 8. Measurement of the global solar radiation – empty square – at left and optical depth – filled circle – at right as a function of the time along the year.

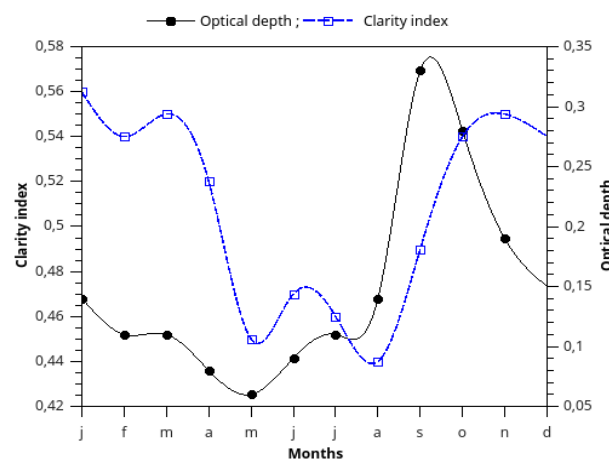


Figure 9. Measurement of the clarity index – empty square – at left and optical depth – filled circle – at right as a function of the time along the year.

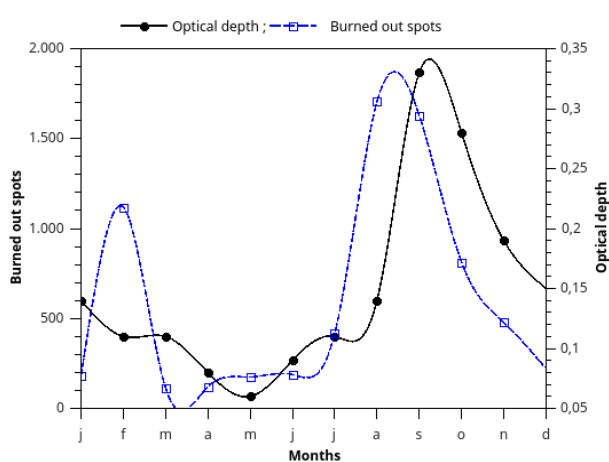


Figure 10. Measurement of the number of wildfires spots – empty square – at left and optical depth – filled circle – at right as a function of the time along the year.

Changes in atmospheric circulation patterns such as high evapotranspiration rates, low average wind speeds, incipient precipitation, and low air humidity favour the elevation of temperatures, indicating the beginning of summer. Another analysis that can be done from the average temperatures is that the thermal amplitudes observed between the months with higher and lower temperatures are very low, varying 4.0 °C in average, between June (lower thermal averages) and October (warmer month).

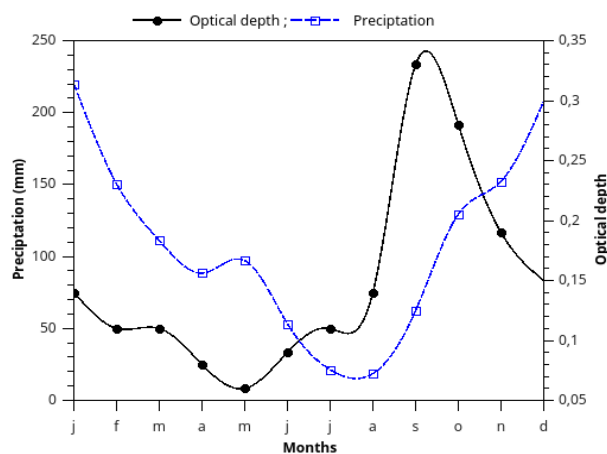


Figure 11. Measurement of the precipitation index – empty square – at left and optical depth – filled circle – at right as a function of the time along the year.

The rainy season goes from October to March/April and accounts for more than 85 % of annual rainfall, with the rains in December and January corresponding for more than 35% of the whole total. The dry season, which starts in April and lasts until the beginning of October, has a significant reduction in rainfall indices. The driest quarter of the year, from June to August, the rainfall represents, on average, less than 2 % of the annual total.

The dry season is characterized by long periods without rainfall or insignificant precipitations, well below the daily evapotranspiration (*ETP*), implying that the condition of environment dryness is not improved. These periods often exceed 100 days. For sake of analysis, periods of drought are defined as those which over 75 days remain without precipitation. During the period of study, there were many longer periods of drought above the minimum limit set. Considering the years for which longer periods of drought have been observed, the average number without rain is 105 days, the average number of days without significant precipitation (below than 2.5 mm) is 110 days. Practically half of the total number of years present long periods without rain exceeding 75 uninterrupted days. These periods coincide with the dry season of the year, being more common during June, July and August.

The variation of the aerosol concentrations in the atmosphere of Campo Grande - MS is strongly influenced by the biomass burning. The practice of biomass burning is related to the meteorological conditions observed during the second winter half and the first spring half. The long period without precipitation and relatively low relative humidity are meteorological factors that contribute to the seasonality of biomass burning (figure 1 on burning outbreaks).

The seasonality of the atmosphere contamination by aerosols for Campo Grande – MS has been verified. Critical periods occur typically between August and October, coinciding with the dry season. The values of the monthly averages of the optical thickness in the channel of 500 nm ($\tau_{500\text{nm}}$) began rising on August ($\tau_{500\text{nm}} \sim 0.1$). Maximum values usually occur in September ($\tau_{500\text{nm}} \sim 0.5$ to 1.0) and decrease from October onwards with the onset of the rainy season. The decrease of the aerosol concentrations in the atmosphere due to the beginning of the rainy season varies from year to year.

The principal events associated with the most intense attenuation of aerosol radiation due to the decreasing number of heat sources have also been detected by the AVHRR/NOAA sensor and the movement analysis by the MODIS/TERRA sensor. The effect of aerosol reduction in the atmosphere due to the beginning of the rain season differs from year to year. The observed and analysed results indicate that some regions are can be considered the main contributors to the presence of aerosols in the atmosphere of Campo Grande - MS (Figure 9 - optical depth and clarity index).

DISCUSSION

To understand the temporal variation of aerosols in the studied area, the time series profile of the mean AOT values are presented in Figures 1 to 11. During the period of study, every maximum AOT value appeared during the spring, i.e. between October and December. The seasonal mean value of $\tau_{500\text{nm}}$ measures how the cyclical variations are different. In 2007 and 2010, seasonal mean values of $\tau_{500\text{nm}}$ showed a downward trend from spring to winter (July ~ September of the following year). Conversely, in 2008 and 2009, these measured values decreased from spring to autumn (April ~ June) and then increased slightly during the winter.

The annual cycle of seasonal averages shows a trend, which decreases first from May to October and then increases from November to April of the following year, and all maximums appear during the spring. Thus, in order to better understand these dissimilar cyclical variations, it is necessary to analyse the spatial and temporal variations of AOT. In all figures from 1 to 12, mean values of $\tau_{500\text{nm}}$ reach the highest during the spring, compared to the rest of the year.

Studies suggest that spring dust and local biomass firing activities in the north of the country may have caused an increase in the aerosol load in this area.^{10,11,28-31} In addition, vast areas of agricultural lands are located in the vicinity of Campo Grande. After the spring harvest, local agricultural wastes (e.g. cane straw, corn, wheat straw and residual wood) are commonly burned to remove unwanted biomass and to control invasive pests.

Thus, biomass burning in late spring and early summer are expected to significantly increase *PREC*, *TEM* and *RHU* values which are all at the highest levels during the summer. High *TEM* and *RHU* can cause the gas-to-particle conversion process resulting in a larger volume of fine particles, and *PREC* can easily remove coarse particles.³²⁻³⁴

Understandably, the increased deposition of coarse particles by precipitation elimination plays a dominant role. For the city of Campo Grande – MS, the population density may be considered medium. The agricultural productivity is pre-eminent and the winter is not very rigorous. The consumption of fossil fuels and biofuels are naturally large, contributing to SO₂ emissions with a mean of 1.76 ppb, varying from a minimum of zero and a maximum of 46.6 ppb during the year.²⁹ The heavily emitted SO₂ can be largely converted to sulfate aerosols in the atmosphere, making it the dominant component of aerosols in Campo Grande.

Sulfates are hygroscopic aerosols, while the size of their particle can grow with increasing humidity. The climate in Campo Grande, characterized by high humidity throughout the rainfall season, may be favourable for the growing single-spreading albedo (SSA) of sulfate aerosols. The SSA aerosol of sulfate doubles when RHU increases.³⁵ Thus, in Campo Grande, the meteorological conditions could contribute approximately equally with heavy emissions of SO₂ to increase the concentrations of particulate material, thus increasing the optical thickness. In addition, Campo Grande is located in a surrounding depression that prevents the horizontal dispersion of concentrated aerosols. Thus, the combined effects of heavy emissions, special weather conditions and negative relief forms can result in high AOT values.

Also, the fuel consumption of human activities in the city of Campo Grande, such as industrial production, heating, depletion of vehicles and daily life, releases waste gases with a large amount of AOT. In addition to the high RHU contributions, it can clearly increase the hygroscopicity of aerosol particles and reduce the dispersion of secondary pollutants, which can result in a larger increase in AOT.

Aerosols and meteorological factors

The temporal variations of AOT are affected mainly by the seasonal variations of the meteorological conditions and emissions of particulate material. Meteorological conditions affect AOTs in different ways, TEM and RHU affect the production of secondary particles,^{30,34} PREC affects deposition³⁴ and velocity affects dispersion.²⁰ In addition, changes in emissions of natural and anthropogenic particles are also closely related to weather conditions. Aerosols also have a considerable impact on atmospheric energy balance and weather conditions. Thus, to better understand the aerosol-meteorological interactions, the statistical properties of AOTs and meteorological factors shall be presented and discussed below.

AOT and meteorological variables

Using the Principal Component Analysis (ACP) extraction method with Varimax rotation and Kaiser normalization, and Cluster analysis obtained by the WARD method, two groups were obtained that explained 87.8 % of the total variance. This total is composed by the factor 1/group 1, which explains 51 % of the variance, and the factor 2/group 2, which explains 36.8 % of the variance.

Cluster analysis was performed, and the results show two separate groups, and within each group there are two

subgroups. They are, for group 1: subgroup 1.1 – ozone and carbon monoxide; subgroup 1.2 – outbreaks of burning. For group 2: subgroup 2.1 – average, maximum and minimum atmospheric pressure, maximum, minimum and average temperatures, and solar radiation; and subgroup 2.2 – mean dew point, maximum and minimum precipitation, maximum and minimum air humidity, clarity index, wind speed, and wind direction.

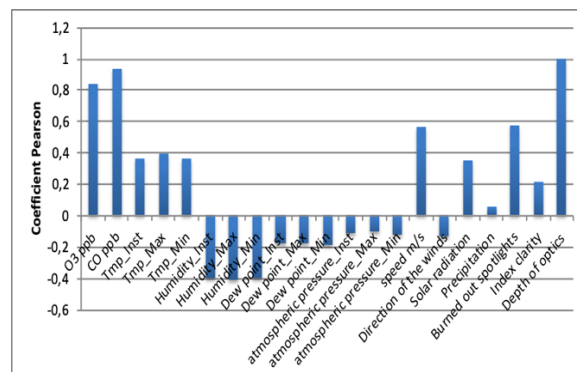


Figure 12. Pearson coefficients relating the studied variables and aerosols for Campo Grande – MS, Brazil.

No obvious relationship was found between AOT and meteorological variables. This may occur because the low-pressure climate is conducive to controlling the dilution and diffusion of air pollution, which plays a significant role in reducing pollution levels. In contrast, under high pressure conditions, higher concentrations of soil-level pollution have been observed in some scientific communications.^{36,37}

The TEM is similar to the AOT pattern, which correlated positively. The next factor, RHU, shows a negative correlation. The PREC indicates a positive correlation. Thus, these results make it clear that high TEM and RHU may result in the increase of fine particles, and PREC can easily remove coarse particles, which are quite similar to the results of some recent published studies.³²⁻³³

During the summer and fall, TEM, RHU and PREC are all larger, resulting in relatively low AOT values. Conversely, during the spring and winter, TEM, RHU and PREC are all smaller, resulting in relatively higher AOT values. Continuing with EVP and SSD, the evaporation capacity is positively correlated with the duration of sunlight. In this study, the seasonal variations of EVP are also consistent with those of SSD and show approximately negative correlations with AOT. This indicates that reductions in evaporation and duration of sunlight seem to be related to rises in aerosol load, which is quite similar to earlier results.^{23,38}

The seasonal mean of AOT is correlated to PRS, TEM, RHU and PREC, as fine particle aerosols are easier to accumulate when all four meteorological factors are at maximum.^{32,33,36} This is due to the fact that aerosols of coarse particles can be easily removed by wet deposition and can result in the reduction of solar radiation that reaches the surface and reduces evaporation.^{23,34,38}

The weighting coefficients are produced using the Principal Component Analysis (PCA) that is used to generate the new PC variables. The first line of values is the amount of variation (%) explained by the corresponding PC variable.

Table 1. Weight coefficients of the new PC variables.

Variables	PC1	PC2
<i>AOT</i>	-0.029	-0.607
Dew point	0.375	0.059
Atmospheric pressure (hPa)	-0.311	-0.242
Solar radiation (MJ m ⁻²)	0.531	0.319
O ₃ ppb	-0.260	0.356
CO ppb	-0.216	0.390
<i>M_m</i>	0.340	0.126
<i>T_{max}</i> C°	0.433	0.159
Humidity _{Max} %	0.341	-0.123
Wind speed (m s ⁻¹)	-0.334	0.197
Direction of winds (degrees)	-0.362	0.063
Clarity index	0.329	0.230
Wildfire spots	-0.212	0.321
Proportion	0.510	0.368
Cumulative	0.510	0.878

PCA Results

New variables with unique physical interpretations were found from PCA data that can be inferred from the weighting coefficients used to create each variable (Table 1). The first PC variable (PC1) accounts for 51 % of the total variance and is derived mainly from the predominant meteorological factors. Positive values of PC1 were obtained for vapour pressure, precipitation, temperature, and humidity. In addition, PC1 also receives negative weights of atmospheric pressure and wind speed. Thus, it can be inferred that the positive values of PC1 are clearly indicative of atmospheric conditions in which the low pressure, the air dryness and the longer duration of the insolation are more likely to occur. Such atmospheric conditions are conducive to controlling the dilution and diffusion of fine particles, which results in relatively low *AOT* – negative values.

The PC2, which represents 36.8 % of the total variance, reveals a more interesting interaction between the pollutant and aerosol variables. In particular, the positive sign of the ozone coefficient is consistent with carbon monoxide because the weighting coefficients obtained for them are almost equal. Thus, the positive values of PC2 correspond to high values of ozone and CO, which play an important role in increasing *AOT*.

If the data are correlated, the model should be adjusted taking into account these auto correlations. This correction is done by inserting the residue into the model. All considerations on temporal trends should be observed when conducting a study, for example, on the impact of a particular variable. Other factors that are generally considered in these studies are the effects of temperature, precipitation and humidity. After considering the mentioned factors, the values of the coefficients, β , are determined. For the group 1, the values of regression analysis yielded the following results.

$$AOT = 0.0643 - 0.00133 O_3 + 0.000446 CO - 0.000006 \textit{wildfires} \quad (8)$$

The O₃ and CO-concentrations are expressed in ppb. The statistical parameters are $S = 0.0217283$, $R - Sq = 96.1 \%$, $R - Sq(\text{adj}) = 92.8 \%$ and error = 0.02.

For the group number 2 the regression analysis resulted in the following equation.

$$AOT = -3.9 + 0.0033 PRS - 0.000011 R_g - 0.00088 PREC + 0.0047 TEM_{\max} + 0.00279 RHU_{\max} + 0.0987 WSP + 0.000413 WDI + 0.383 K_t \quad (9)$$

In this equation, the pressure (*PRS*) is measured in hPa, radiation (*R_g*) in MJ m⁻², precipitation (*PREC*) in mm, temperature (*TEM*) in °C, humidity (*RHU*) in %, wind speed (*WSP*) in m s⁻¹, wind direction (*WDI*) in angular degrees and the clarity index as the number defined by Eqn. (1). The resulting statistical parameters are $S = 0.0735384$, $R - Sq = 70.2 \%$, $R - Sq(\text{adj}) = 17.9 \%$ and error = 0.37.

The incidence of solar radiation causes the heating of the surface and initiates convective processes that cause the variation in aerosol concentration through turbulent movements. These variations are responsible for the raise or reduction in aerosol concentration within a certain volume from both horizontal and vertical motion.

Environmental degradation is one of the main problems of modern society. Technological development, population growth and its concentration in the urban environment, industrialization and the use of new methods and techniques in agriculture are some of the contributing factors for the introduction of different chemical, synthetic and even natural substances into the environment, which generate adverse effects on the environment and living things.

CONCLUSION

The local averages of seasonality, considering the crests and depressions of the curve, indicating the increased concentration of aerosols observed during the analysis can be attributed: (i) to the dust aerosols produced locally from desert zones and catalyzed by intense solar heating also as transported aerosols; (ii) to the increase in anthropogenic activities, as the land preparation and biomass burning that release a significant amount of dust and smoke particles into the atmosphere; (iii) to the smoke particles transported from neighbouring countries and neighbouring states – the southern part of Campo Grande is called the arc of fire, region where there is a higher incidence of wildfires; and (iv) to the atmospheric inversion condition prevalent in the region, which does not withstand upward movement of air resulting in high aerosol loading at the lower levels of the atmosphere. The low *AOT* observed during the local moist months can be attributed to the reduction of anthropogenic activities and the increase of wet deposition processes.

It is known that precipitation directly influences the aerosol load. The reverse modal patterns between precipitation and *AOT* (see Figure 11) indicate the role played by precipitation in modulating the *AOT* concentration. The stations with high (low) precipitation correspond to *AOT* valleys (peaks). This is further evidenced by significant negative correlation (with

95 % confidence level) between *AOT* and precipitation (Figure 12). Generally, precipitation can affect aerosol loading, especially dust particles in different ways: (i) it washes aerosols by reducing their concentration in the atmosphere, a process known as elimination; (ii) increases soil moisture by suppressing induced dust emissions as winding the ground. In addition, it increases the growth of the vegetation, which could also prevent the emission of dust. However, during periods of drought, the residue varies freely due to the aerosol emissions from burnings and biomass events.

In this study, the aerosol and meteorological data were analysed to assess the relationships between aerosols and meteorological conditions. The aerosol distribution properties have first been examined in the research area and found that the temporal variations of the *AOT* show different characteristics and are mainly affected by variations in meteorological conditions and particulate emissions. A main result of this work is that the seasonal annual cycle of *AOT* shows a decreasing trend followed by a rise, and all highs appear in the spring.

The variability of *AOT* in the 500 nm channel verified in the atmosphere of Campo Grande – MS presents a strong monthly seasonality related to the predominant meteorological conditions and to the numerous fires of burnings verified in regions that are source of aerosols. In the months with the greatest influence of the wildfires, monthly averages of $\tau_{500\text{nm}}$ from 0.6 to 1.0 were observed, while in the months with cleaner atmosphere values of $\tau_{500\text{nm}}$ were observed around 0.1. The mathematical correlation between the climatic indicators indicated that the main source in order of significance formed two groups, with two subgroups each.

The analysis of the temporal variability of *AOT* showed that Campo Grande has a characteristic annual cycle with increase of *AOT* in the periods of August to October, with maximums recorded in the month of September, coinciding with the period of increase of burnings in the southern Amazon and in the areas of the Brazil Central-West “cerrado”, while in the other months of the year *AOT* has low values, around 0.1.

It was observed that the years presenting the highest *AOT* load in the region were those in which there were a greater number of outbreaks of burning in the Brazilian territory. The atmospheric circulation and frontal systems that operate in South America during the dry season period interfere in the amount of foci and, consequently, in the *AOT* values for several regions, including Campo Grande, which is one of the places, affected by the air masses that aerosol from the northern region.

FUNDING

This research received no external funding. Flavio Aristone is thankful to CNPq for financial support.

ACKNOWLEDGMENTS

The authors thank their Universities for their support.

DATABASE STATEMENT/DATA AVAILABILITY

The climate database is public domain and available at: INMET: http://www.inmet.gov.br/portal/index.php?r=_estacoes/estacoesAutomaticas; <https://giovanni.gsfc.nasa.gov/giovanni>; <http://climan.alise.cptec.inpe.br/~rclimanl/boletim/>

REFERENCES

- Chen, S., Zhao, C., Qian, Y., Leung, L. R., Huang, J.-P., Huang, Z.-W., Bi, J.-R., Zhang, W., Shi, J.-S., Yang, L., Li, Deshuai, Li, J. X., Regional modeling of dust mass balance and radiative forcing over East Asia using WRF-Chem, *Aeolian Res.*, **2014**, *15*, 15–30. <https://doi.org/10.1016/j.aeolia.2014.02.001>
- Gui, Ke; Che, Huizheng; Chen, Quanliang; Zeng, Zhaoliang; Zheng, Yu; Long, Qichao; Sun, Tianze; Liu, Xinyu; Wang, Yaqiang; Liao, Tingting; Yu, Jie; Wang, Hong; Zhang, Xiaoye. Water vapor variation and the effect of aerosols in China, *Atm. Environ.*, **2017**, *165*, 322–335. DOI: 10.1016/j.atmosenv.2017.07.005
- Brock, C. A., Cozic, J., Bahreini, R., Froyd, K. D., Middlebrook, A. M., McComiskey, A., Brioude, J., Cooper, O. R., Stohl, A., Aikin, K. C., de Gouw, J. A., Fahey, D. W., Ferrare, R. A., Gao, R.-S., Gore, W., Holloway, J. S., Hübler, G., Jefferson, A., Lack, D. A., Lance, S., Moore, R. H., Murphy, D. M., Nenes, A., Novelli, P. C., Nowak, J. B., Ogren, J. A., Peischl, J., Pierce, R. B., Pilewskie, P., Quinn, P. K., Ryerson, T. B., Schmidt, K. S., Schwarz, J. P., Sodemann, H., Spackman, J. R., Stark, H., Thomson, D. S., Thornberry, T., Veres, P., Watts, L. A., Warneke, C., and Wollny, A. G.: Characteristics, sources, and transport of aerosols measured in spring 2008 during the aerosol, radiation, and cloud processes affecting Arctic Climate (ARCPAC) Project, *Atm. Chem. Phys.*, **2011**, *11*, 2423–2453, <https://doi.org/10.5194/acp-11-2423-2011>.
- Qian, Y. U. N., Leung, L. R., Ghan, S. J., Giorgi, F., Regional climate effects of aerosols over China: Modeling and observation, *Tellus B Chem. Phys. Meteorol.*, **2011**, *55(4)*, 914–934. doi.org/10.3402/tellusb.v55i4.16379
- Levy H, Horowitz L, Schwarzkopf M, Ming Y, Golaz J, Naik V, Ramaswamy V. The roles of aerosol direct and indirect effects in past and future climate change, *J. Geophys. Res. Atmos.*, **2013**, *118(10)*, 4521–4532. doi.org/10.1002/jgrd.50192
- Gao, Y., Liu, X., Zhao, C., Zhang, M., Emission controls versus meteorological conditions in determining aerosol concentrations in Beijing during the 2008 Olympic Games, *Atm. Chem. Phys.*, **2011**, *11*, 16655–16691. DOI: 10.5194/acpd-11-16655-2011
- Zhang, Z., J. Wang, L. Chen, X. Chen, G. Sun, N. Zhong, H. Kan, and W. Lu. Impact of haze and air pollution-related hazards on hospital admissions in Guangzhou, China. *Environ. Sci. Pollut. Res.*, **2014**, *21*, 4236–4244. [doi: 10.1007/s11356-013-2374-6](https://doi.org/10.1007/s11356-013-2374-6)
- Lu F, Xu D, Cheng Y, Dong S, Guo C, Jiang X, Zheng X, Systematic review and meta-analysis of the adverse health effects of ambient PM2.5 and PM10 pollution in the Chinese population, *Environ. Res.* **2015**, *136*, 196–204. [doi: 10.1016/j.envres.2014.06.029](https://doi.org/10.1016/j.envres.2014.06.029).
- Mukherjee, A., Agrawal, M., World air particulate matter: sources, distribution and health effects, *Environ. Chem. Lett.*, **2017**, *15(2)*, 283–309.
- Souza, A. Santos, D. A. S., Lariane, P. G. C., Poluição Atmosférica Urbana A Partir De Dados De Aerossóis Modis: Efeito Dos Parâmetros Meteorológicos, *Boletim Goiano de Geografia*, **2017**, *37*, 466. doi.org/10.5216/bgg.v37i3.50766
- Souza, A., Ihaddadene, R., Ihaddadene, N., Oguntunde, P. E., Clarity Index Analysis and Modeling Using Probability Distribution Functions in Campo Grande-MS, Brazil, *J. Sol. Energy Eng.*, **2019**, *141(6)*, 061001. <https://doi.org/10.1115/1.4043615>

- ¹²Steiner, W. A., The influence of air pollution on moss-dwelling animals, I. Methodology and composition of flora and fauna, *Rev. Suisse Zool.*, **1994**, *101*(2), 533–556. <https://doi.org/10.5962/bhl.part.79917>
- ¹³Shang, H., Chen, L., Tao, J., Lin, S., Jia, S., Synergetic use of MODIS cloud parameters for distinguishing high aerosol loadings from clouds over the North China Plain. *IEEE. J. Sel. Top. Appl. Earth Obs. Remote Sens.*, **2014**, *7*(12), 4879–4886. DOI: [10.1109/JSTARS.2014.2332427](https://doi.org/10.1109/JSTARS.2014.2332427)
- ¹⁴Zhang Z., Wu W., Wei J., Song Y., Yan X., Zhu L., Wang Q., Aerosol optical depth retrieval from visibility in China during 1973–2014, *Atm. Environ.*, **2017**, *171*, 38–48. DOI: [10.1016/j.atmosenv.2017.09.004](https://doi.org/10.1016/j.atmosenv.2017.09.004)
- ¹⁵Che, H., Zhang, X.-Y., Xia, X., Goloub, P., Holben, B., Zhao, H., Wang, Y., Zhang, X.-C., Wang, H., Blarel, L., Damiri, B., Zhang, R., Deng, X., Ma, Y., Wang, T., Geng, F., Qi, B., Zhu, J., Yu, J., Chen, Q., and Shi, G., Ground-based aerosol climatology of China: aerosol optical depths from the China Aerosol Remote Sensing Network (CARSNET) 2002–2013, *Atm. Chem. Phys.*, **2015**, *15*(13), 7619–7652. <https://doi.org/10.5194/acp-15-7619-2015>
- ¹⁶Filonchik, M., Yan, H., Zhang, Z., Analysis of spatial and temporal variability of aerosol optical depth over China using MODIS combined Dark Target and Deep Blue product, *Theor. Appl. Climatol.*, **2018**, 1–18, <https://doi.org/10.1007/s00704-018-2737-5>.
- ¹⁷Sarkar, T., Mishra, M., Soil Erosion Susceptibility Mapping with the Application of Logistic Regression and Artificial Neural Network. *J. Geovis. Spat. Anal.*, **2018**, *2*(1), 8. <https://doi.org/10.1007/s41651-018-0015-9>.
- ¹⁸Dawson, J. P., Adams, P. J., Pandis, S. N., Sensitivity of PM_{2.5} to climate in the Eastern US: A modeling case study, *Atmos. Chem. Phys.*, **2007**, *7*(16), 4295–4309, doi:10.5194/acp-7-4295-2007.
- ¹⁹Dawson, J. P., Racherla, P. N., Lynn, B. H., Adams, P. J., Pandis, S. N., Impacts of climate change on regional and urban air quality in the eastern United States: Role of meteorology, *J. Geophys. Res.*, **2009**, *114*, D05308, doi:10.1029/2008JD009849.
- ²⁰Deng, X., Shi, C., Wu, B., Chen, Z., Nie, S., He, D., Zhang, H., Analysis of aerosol characteristics and their relationships with meteorological parameters over Anhui province in China, *Atm. Res.*, **2012**, *109–110*(0), 52–63, doi:10.1016/j.atmosres.2012.02.011.
- ²¹Jiménez-Guerrero, P., Montávez, J. P., Gómez-Navarro, J. J., Jerez, S., Lorente-Plazas, R., Impacts of climate change on ground level gas-phase pollutants and aerosols in the Iberian Peninsula for the late XXI century, *Atm. Environ.*, **2012**, *55*(0), 483–495, doi:10.1016/j.atmosenv.2012.02.048.
- ²²Yang, X., Ferrat, M., Li, Z. Q., New evidence of orographic precipitation suppression by aerosols in central China, *Meteorol. Atm. Phys.*, **2013**, *119*(1–2), 17–29, doi:10.1007/s00703-012-0221-9
- ²³Wang, Y. W., Yang, Y. H., China's dimming and brightening: Evidence, causes and hydrological implications, *Ann. Geophys.*, **2014**, *32*(1), 41–55, doi:10.5194/angeo-32-41-2014.
- ²⁴Latorre, M., Cardoso, M., Análise De Séries Temporais Em Epidemiologia: Uma Introdução Sobre Aspectos Metodológicos, *Rev. Bras. Epidemiol.*, **2014**, *4*(3), 145–152.
- ²⁵Montgomery, D. C., Peak, E. A., *Introduction to linear regression analysis*. 2nd Ed., Wiley, New York, **1992**, 68–79.
- ²⁶Abdi, H., Williams, L. J., Principal component analysis, *WIREs Comp. Stat.*, **2010**, *2*(4), 433–459. doi:10.1002/wics.101.
- ²⁷Jones, T. A., Christopher, S. A., Statistical properties of aerosol-cloud-precipitation interactions in South America, *Atm. Chem. Phys.*, **2010**, *10*(5), 2287–2305, doi:10.5194/acp-10-2287-2010.
- ²⁸Souza, A., Santos, D. A. S., Análise das componentes principais no processo de monitoramento ambiental, *Nativa*, **2018**, *6*, 639. <http://dx.doi.org/10.31413/nativa.v6i6.6453>
- ²⁹Souza, A., Santos, D. A. S., Aristone, F., Kovač-Andrić, F., Marković, B., Matasović, B., Pavao, H. G., Pires, J. C. M., Ikefuti, P. V., Impacto De Fatores Meteorológicos Sobre As Concentrações De Ozônio Modelados Por Análise De Séries Temporais E Métodos Estatísticos Multivariados, *Holos (Natal. Online)*, **2017**, *5*, 2. DOI: <https://doi.org/10.15628/holos.2017.5033>
- ³⁰Souza, A., Ikefuti, P. V., Garcia, A. P., Santos, D. A. S., Oliveira, S., Análise da relação entre O₃, NO e NO₂ usando técnicas de regressão linear múltipla, *Geographia (UFF)*, **2018**, *20*, 124. DOI: 10.22409/geographia.v20i43.1065
- ³¹Souza, A., Jan, B., Nawaz, F., Zai, M. A. K. Y., Oliveira, S. S., Pavao, H. G., Fernandes, W. A., Ihaddadene, R., Ihaddadene, N., Oguntunde, P. E., Santos, D. A. S., Temporal variations of SO₂ in an urban environment, *Discovery*, **2019**, *55*(283), 328–339.
- ³²Lee, K. H., Kim, Y. J., von Hoyningen-Huene, W., Burrow, J. P., Spatio-temporal variability of satellite-derived aerosol optical thickness over Northeast Asia in 2004, *Atm. Environ.*, **2007**, *41*(19), 3959–3973, doi:10.1016/j.atmosenv.2007.01.048
- ³³Che, H. Z., Zhang, X. Y., Alfraro, S., Chatenet, B., Gomes, L., Zhao, J. Q., Aerosol optical properties and its radiative forcing over Yulin, China in 2001 and 2002, *Adv. Atm. Sci.*, **2009**, *26*(3), 564–576, doi:10.1007/s00376-009-0564-4
- ³⁴Tao, J., Zhang, L., Engling, G., Zhang, R., Yang, Y., Cao, J., Zhu, C., Wang, Q., Luo, L., Chemical composition of PM_{2.5} in an urban environment in Chengdu, China: Importance of springtime dust storms and biomass burning, *Atm. Res.*, **2013**, *122*(0), 270–283, doi:10.1016/j.atmosres.2012.11.004.
- ³⁵Thornhill, G. D., Ryder, C. L., Highwood, E. J., Shaffrey, L. C., Johnson, B. T., The effect of South American biomass burning aerosol emissions on the regional climate, *Atm. Chem. Phys.*, **2018**, *18*, 5321–5342. <https://doi.org/10.5194/acp-18-5321>.
- ³⁶Chen, Z. H., Cheng, S. Y., Li, J. B., Guo, X. R., Wang, W. H., Chen, D. S., Relationship between atmospheric pollution processes and synoptic pressure patterns in northern China, *Atm. Environ.*, **2008**, *42*(24), 6078–6087. doi:10.1016/j.atmosenv.2008.03.043.
- ³⁷Im, U., Tayanc, M., Yenigun, O., Analysis of major photochemical pollutants with meteorological factors for high ozone days in Istanbul, Turkey, *Water Air Soil Pollut.*, **2006**, *175*(1–4), 335–359. doi:10.1007/s11270-006-9142-x.
- ³⁸Sanchez-Lorenzo, A., Calbó, J., Wild, M., Azorin-Molina, C., and Sanchez-Romero, A.: New insights into the history of the Campbell-Stokes sunshine recorder, *Weather*, **2013**, *68*, 327–331, doi:10.1002/wea.2156.

Received: 17.05.2020.

Accepted: 18.06.2020.



GLYCEROL MEDIATED ONE-POT SYNTHESIS OF PYRAZOLE CONJUGATED TETRAHYDROQUINOLINE DERIVATIVES AND EVALUATION OF THEIR ANTICANCER ACTIVITY

N. Amarnath Reddy,^[a] K. Kamala,^[b] Raveendra Dayam^[a] and K. V. Saritha^{[c]*}

Keywords: 3-Methyl-1-phenyl-1H-pyrazol-5-amine; 5,5-dimethylcyclohexane-1,3-dione; one-pot reaction; glycerol; anticancer activity.

Pyrazole scaffold is an important building block in many of the medicinally active new chemical entities. In the current work, synthesis of pyrazole conjugated tetrahydroquinoline derivatives has been achieved by treating 3-methyl-1-phenyl-1H-pyrazol-5-amine (**1**), 5,5-dimethylcyclohexane-1,3-dione (**2**), and benzaldehydes (**3**) at 80-85 °C for 60-90 min using glycerol as green reaction medium. The anticancer activity of the synthesized pyrazole-conjugates was carried out on breast cancer (MCF-7) and liver cancer (A549) cell lines. Two among the tested compounds showed potential inhibition on A549 cell lines. Further, molecular modeling studies have performed and the binding interactions with the target protein have been observed. Additionally, pharmacokinetic properties such as bioavailability, log *P*, total polar surface area and blood brain barrier (BBB) have been predicted using SwissADME tools to get insight into the further structural optimization.

* Corresponding Authors

E-Mail: kvsarithasvu@gmail

[a] Excelra Knowledge Solutions Private Limited, IDA Uppal, Hyderabad-500 039, India

[b] Department of Bio-Technology, Rayalaseema university, Kurnool, Andhra Pradesh, India

[c] Department of Bio-Technology, S.V. University, Tirupati, Andhra Pradesh, India

INTRODUCTION

Pyrazolo[3,4-*b*]quinoline derivatives were momentous for their pharmacological activities. In particular, they showed potential anticancer, anti-malarial, antiviral, and anti-inflammatory properties.¹⁻³ These are also known for parasiticidal properties, antibacterial, antitumor, hypotensive, and vasodilation activities.¹⁻³ In specific, pyrazolo-annulated heterocyclic scaffold is being found in a diverse therapeutic drugs such as COX inhibitors, Phosphodiesterase 5 (PDE5) inhibitor (Sildenafil Citrate - Viagra), and mTOR signaling inhibitors (WYE-354) (Figure 1) etc.⁴ Due to their growing importance, various synthetic protocols have been reported in the recent past for the preparation of pyrazolo[3,4-*b*]quinoline scaffolds using different homogeneous and heterogeneous materials such as FeNi₃-ILs,⁵ PEGOSO₃H,⁶ L-proline,⁷ and InCl₃⁸ as catalysts. However, the aforementioned methods have limitations and suffer from drawbacks such as prolonged reaction times, harsh reaction conditions, catalyst separation challenges, tedious workup, waste generation, toxic solvents, high reaction temperatures and low product yields. Therefore, there is a pressing need for newer methods that could surmount the above challenges.

Research for finding other alternate reaction media, which can substitute the hazardous, toxic, and inflammable organic solvents, which pose a serious threat to the environment, is gaining progress. Many environmentally compatible reaction media like green solvents,⁹ ionic liquids,¹⁰

supercritical fluids,¹¹ and fluoros phases,¹² are being used for several organic reactions. Each has its own advantages and is dependent on external factors like lipophilicity, pressure, and viscosity.

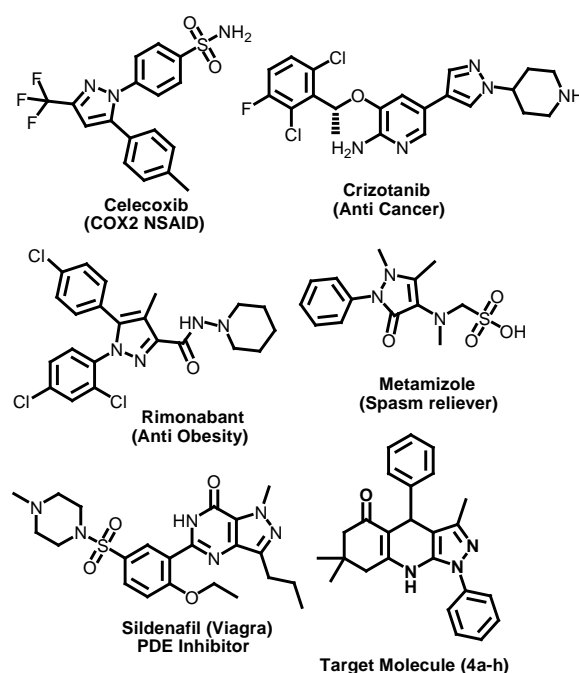


Figure 1. Some therapeutically active compounds containing pyrazole scaffold.

Glycerol was an environmental and biodegradable solvent produced as a by-product in the biodiesel industry¹³. Given the high boiling point property of glycerol, reactions using this as a medium can be carried out at high temperature, thus allowing acceleration of the reaction or making possible reactions that do not proceed in low boiling point solvents.

Table 1. Optimization of reaction conditions for the synthesis of **4a**.

S. No.	Solvent	Temp. °C	Catalyst	Time h	Yield %
1	Glycerol	80-85	TEA, 1 equiv.	1	90
2	Ethylene glycol	80-85	TEA, 1 equiv.	2	80
3	DMF	80-85	TEA, 1 equiv.	2	60
4	DMSO	80-85	TEA, 1 equiv.	2	65
5	Glycerol	80-85	Piperidine, 1 equiv.	1.5	85
6	Ethylene glycol	80-85	Piperidine, 1 equiv.	2.5	81
7	DMF	80-85	Piperidine, 1 equiv.	3	65
8	DMSO	80-85	Piperidine, 1 equiv.	3	68
9	Glycerol	80-85	DBU, 1 equiv.	1.5	87
10	Ethylene glycol	80-85	DBU, 1 equiv.	2.5	83
11	DMF	80-85	DBU, 1 equiv.	2.5	68
12	DMSO	80-85	DBU, 1 equiv.	2.5	69
13	Glycerol	60-65	TEA, 1 equiv.	5	88
14	Glycerol	90-95	TEA, 1 equiv.	1	87
15	Glycerol	80-85	TEA, 0.5 equiv.	1.5	86
16	Glycerol	80-85	TEA, 2 equiv.	1	85

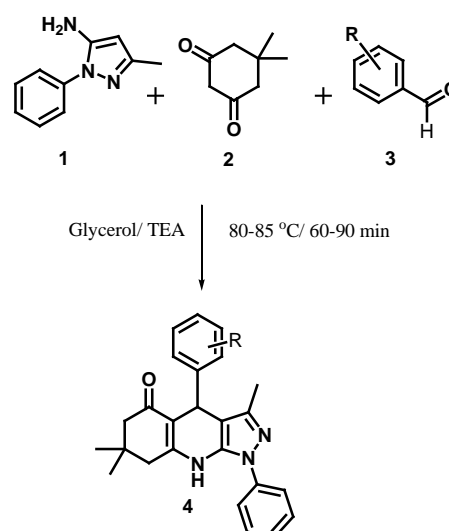
In the bulk manufacturing of active pharmaceutical ingredients (API), the low toxicity of glycerol allows to be used as a solvent in the synthesis of in which the toxicity and residue of solvent have to be carefully controlled. Due to the unique physico-chemical properties, there are a large number of reports on the applications of glycerol as efficient and convenient solvents in organic transformations.¹³

In view of the importance of pyrazole scaffold, we report presently an efficient one-pot protocol for the synthesis of pyrazolo[3,4-*b*]quinolines using glycerol as green reaction medium. There have been no earlier reports for the preparation of pyrazolo[3,4-*b*]quinoline derivatives in glycerol as solvent.

RESULTS AND DISCUSSION

Initially, using the one-pot three-component reaction of 3-methyl-1-phenyl-1*H*-pyrazol-5-amine (**1**) (1 mmol) with 5,5-dimethylcyclohexane-1,3-dione (**2**) (1 mmol), and benzaldehyde (**3a**) (1 mmol) was carried out at 80-85 °C as a model for synthesis of 3,7,7-trimethyl-1,4-diphenyl-6,7,8,9-tetrahydro-1*H*-pyrazolo[3,4-*b*]quinolin-5(4*H*)-one (**4a**). We examined the suitable solvents like glycerol, ethylene glycol, DMSO and DMF at different temperature in the presence of 1 equiv. TEA as catalyst at 80-85 °C. Results are summarised in Table 1. It is observed that the formation of **4a** by one-pot three component reaction in glycerol at 80-85 °C for 60 min gave excellent yield 90 % compare to other conditions (Table 1 entry 1). The structure of **4a** was confirmed by ¹H, ¹³C-NMR, and Mass spectroscopy.

Further, optimization studies were carried out by altering different catalysts such as piperidine and DBU for formation of **4a** by using **1**, **2** and **3a**. It is noticed that usage of piperidine and DBU as catalyst for this reaction resulted in low yields (Table 1, entry 5 and 12). Lower and higher temperature also gave low yield in formation of **4a** (Table 1, entry no 13 and 14).

**Scheme 1.** Synthesis of **4a-4h** by one-pot synthesis.

In the continuous efforts to optimize the one-pot three component reaction, different catalyst amounts were used like 0.5 equiv., 1 equiv. and 2 equiv. of TEA and consistent optimized results were obtained with 1 equiv. of TEA. Results were summarised in Table 1 (Entry no 1, 15 & 16). However, finally formation of **4a** in glycerol as solvent at 80-85 °C in the presence of 1 equiv. of TEA gave excellent yield for 60 min. Having optimised one-pot three component reaction conditions, we explored the scope and limitations with series of substituted anilines **3a-3h**. It was found that the both electron-deficient and electron-rich anilines were applicable for this optimised conditions affording the corresponding benzothiazole derivatives yields 85-90 % (Figure 2). Encouraged by these results, the synthesis of **4a-4h** were carried out in one-pot three component reaction by using **1**, **2** and **3a-3h** in glycerol at 80-85 °C in the presence of 1 equiv. TEA for 60-90 min (Scheme 1) with excellent yields of 85-90 %. Structures were confirmed by ¹H and ¹³C NMR, and mass spectroscopy.

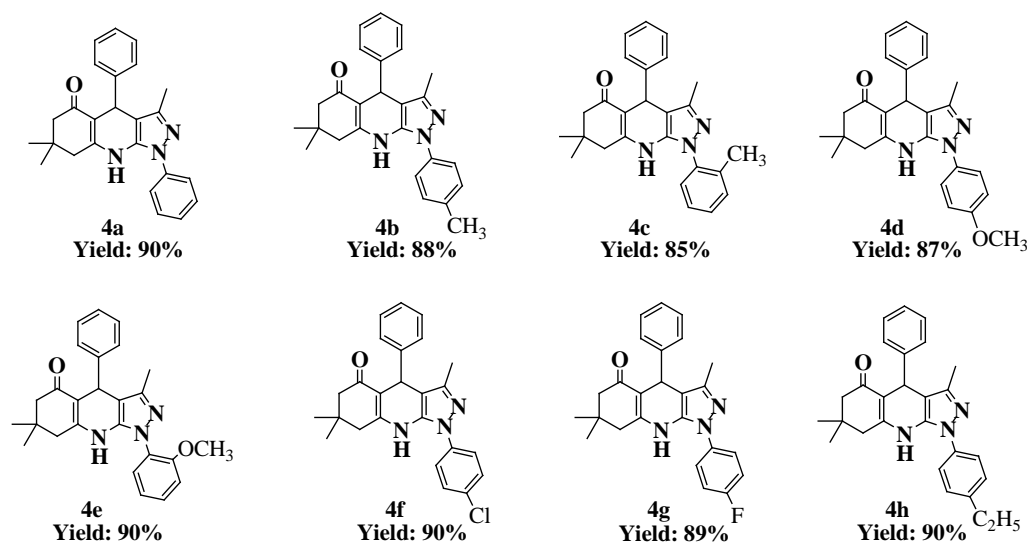


Figure 2. Structures and yields of **4a-h** synthesized by the one-pot reaction.

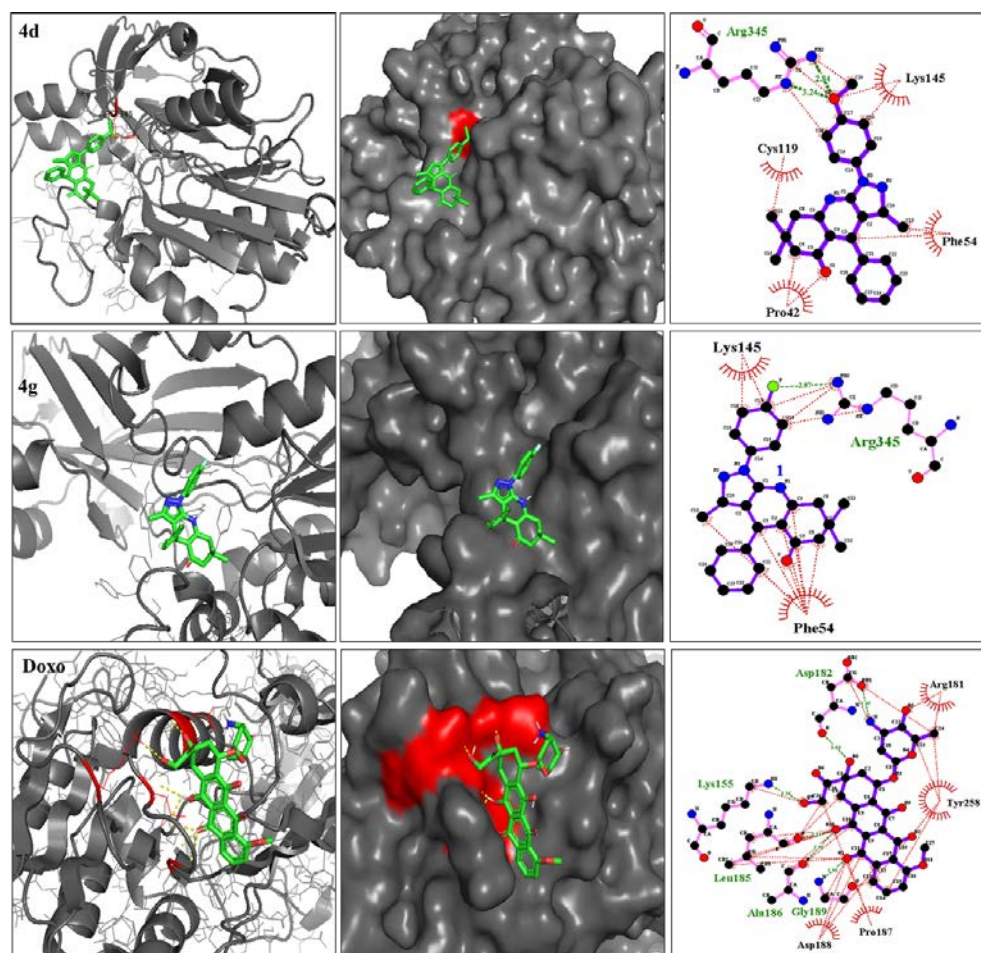


Figure 3. Molecular interactions of human Type I protein arginine methyltransferases (PRMTs) with different test compounds **4d**, **4g** and Doxorubicin. The interactions for the best docked pose for each ligand was showed in the image. The amino acids interacted with the docked ligands are illustrated using LigPlot.

Cytotoxicity assay

A series of 8 conjugates were synthesized and evaluated for their cytotoxicity against two different human cancer cell lines (A549 and MCF7) using MTT assay. IC₅₀ values of the compounds against different cancer cell lines were tabulated and shown in the table 2. Some of the compounds showed substantial reduction in the cell viability of cancer cells in a dose dependent manner. Compound **4d** and **4g** showed good activity against A549 cells with an IC₅₀ value of 9.3 and 9.6 μM, respectively.

Table 2. Cytotoxicity of the synthesized compounds, screened against MCF-7 and A549 cell lines using MTT assay.

Compound	IC ₅₀ value in μM (Mean ± S.D.)	
	MCF-7	A549
4a	>100	>100
4b	14.3 ± 0.43	16.7 ± 0.22
4c	>100	>100
4d	12.4 ± 0.38	9.3 ± 0.18
4e	14.6 ± 0.42	9.8 ± 0.38
4f	24.6 ± 0.35	19.6 ± 0.26
4g	7.9 ± 0.12	9.6 ± 0.16
4h	21.4 ± 0.46	17.5 ± 0.27
Doxorubicin (Positive control)	0.68 ± 0.05	8.63 ± 0.04 nM

Molecular docking

The selected compounds (**4d** and **4g**) from the preliminary screening were evaluated for *in silico* docking analysis. Molecular docking for the compounds **4d** and **4g** was performed against the human Type I protein arginine methyltransferases (PRMTs) active site. A total of ten different conformations were examined for each docked ligand. The binding energies for the best-docked pose of **4d** and **4g** compounds in the receptor active site were -8.2 and -8.0 kcal mol⁻¹, respectively. Whereas the positive control Doxorubicin showed -8.4 kcal/mol.

Table 3. The binding energies, RMSD values and amino acids in the receptor protein interacted with ligands were determined using autodock and LigPlot.

Ligand	Binding energy (kcal mol ⁻¹)	RMSD	H-bond/s	Protein-Ligand interactions
4d	-8.2	3.813	Arg345	Pro42, Phe54, Cys119, Lys145
4g	-8.0	4.853	Arg345	Phe54, Lys145
Doxorubicin (Positive control)	-8.4	2.544	Lys155, Asp182, Leu185, Ala186, Gly189	Arg181, Asp188, Pro187, Tyr258

The interactions between protein and ligands were majorly influenced by hydrophobic and hydrogen bonding interactions. The best docking poses were represented in the Figure 2 and the resulting binding energies along with RMSD values were shown in Table 3. Further, the amino acids interacted with the ligands were shown in the **Table 3**.

Pharmacokinetic properties prediction

Pharmacokinetic properties are crucial to know how human body reacts to a drug molecule. The ADME parameters such as absorption, distribution, metabolism, and excretion are important features for a potential drug molecule.¹⁴ SwissADME tool gives the information about different pharmacokinetic properties such as Human gastrointestinal absorption (HIA), blood-brain-barrier (BBB) permeability, total polar surface area (TPSA) and bioavailability score, etc. TPSA score helps to predict the oral bioavailability of the compounds. The compounds with less TPSA score ranging between 20 and 130 Å have high oral bioavailability.

In the present study all the synthesized molecules exhibited high oral bioavailability. BOILED-Egg model was used for the prediction of gastrointestinal absorption.¹⁵ All the compounds in the series exhibited high gastrointestinal absorption (GIA) and blood-brain barrier permeation.^{14,16} Moreover, the results showed that all the compounds are the substrates for P-glycoprotein (Pgp). Thus the compounds are actively transported out of the body system. In addition, the compounds showed 0.55 bioavailability score. Collectively the results of the synthesized molecules exhibited good physiochemical as well as good pharmacokinetic properties.

EXPERIMENTAL

Melting points were determined in open capillary tubes in sulphuric acid bath. FT-IR spectra are recorded on a VERTEX 70 Bruker by using KBr. A Bruker DRX-400 spectrometer 400 and 100 MHz was employed for recording ¹H NMR and ¹³C NMR spectra respectively and DMSO-d₆ was used as solvent and TMS as an internal standard. Mass spectra were recorded on Agilent-LCMS instrument.

General synthetic procedure

In a typical experiment, a mixture of **1** (1 mmol), **2** (1 mmol), and benzaldehydes **3a-3h** (1 mmol) in 10 mL of glycerol were charged in a 50 mL round bottomed flask and the mixture was stirred at 80-85 °C. The reaction was complete within 60-90 min as analyzed by TLC using petroleum ether/ethyl acetate (60:40) as eluent. The reaction mixture was allowed to cool to room temperature (25-30 °C) and 50 mL of water was added. The precipitate formed was collected by filtration, washed with water and ethanol to afford 90 % of pure 3,7,7-trimethyl-1,4-diphenyl-6,7,8,9-tetrahydro-1*H*-pyrazolo[3,4-*b*]quinolin-5(4*H*)-one derivatives as identified by spectral data.

Cytotoxicity assay

Cytotoxicity of the synthesized compounds was tested against two different human cancer cell lines A549 (Human lung carcinoma) and MCF 7 (Human breast carcinoma) using MTT assay.¹⁷

Molecular Docking

In silico molecular binding of the synthesized compounds **4d** and **4g** with human Type I protein arginine methyltransferases (PRMTs) protein was evaluated using AutoDockTools.¹⁸ Based on cytotoxicity results, the selected ligand structures were generated using Chem3D Ultra 16.0 software. MOPAC (semi-empirical quantum mechanics) tool was used to minimize the energies of the ligand structures and the outcomes were saved in protein data bank (.pdb) format using Chem3D Ultra 16.0 software. The PDB structure of PRMTs protein (PDB ID: 6NT2) was downloaded and imported to the workspace. The Kollman charges were incorporated to the protein and were processed for further in AutoDock. Further, the grid box with a size of 90 in all the axes (X, Y, Z) was generated for the processed protein. The visualization of the output file generated from docking was analysed using PyMol. Doxorubicin was used as a positive control. One pose per run was taken based on RMSD clustering using energy penalty of 100 and the heavy atom threshold set at 1.0 Å. All the poses were examined manually and the best pose was taken. The hydrogen and hydrophobic interactions of the ligand molecules with receptor protein was studied by using LIGPLOT.¹⁹

SwissADME

The physicochemical descriptors, pharmacokinetic properties and *in silico* drug likeliness of the synthesised compounds were predicted by using SWISSADME server. Lipophilicity and polarity of the compounds were predicted by BOILED-Egg (Brain Or Intestinal Estimated permeation) method.^{20,21} Doxorubicin was used as a positive control.

3,7,7-Trimethyl-1,4-diphenyl-6,7,8,9-tetrahydro-1H-pyrazolo[3,4-*b*]quinolin-5(4H)-one (4a)

Yield 90 %, m.p. 191-193 °C. ¹H NMR (400 MHz, DMSO-*d*₆) δ = 1.0 (s, 3H, CH₃), 1.05 (s, 3H, CH₃), 2.0 (s, 3H, CH₃), 2.2-2.4 (d, 4H, CH₂), 5.1 (s, 1H, CH), 6.5 (s, 1H, NH), 7.0-8.0 (m, 10H, Ar-H). ¹³C NMR (100 MHz, DMSO-*d*₆) δ = 12.1, 27.4, 28.3, 29.6, 32.1, 36.1, 41.2, 48.7, 50.7, 104.7, 112.7, 121.5, 125.1, 126.4, 127.3, 127.6, 128.1, 129.2, 135.2, 145.9, 147.9, 195.0. MS: M⁺1 = 384.

3,7,7-Trimethyl-4-phenyl-1-(*p*-tolyl)-6,7,8,9-tetrahydro-1H-pyrazolo[3,4-*b*]quinolin-5(4H)-one (4b)

Yield 88 %, m.p. >220 °C. ¹H NMR (400 MHz, DMSO-*d*₆) δ = 0.9 (s, 3H, CH₃), 1.0 (s, 3H, CH₃), 1.7 (s, 3H, CH₃), 1.9-2.1 (d, 4H, CH₂), 5.1 (s, 1H, CH), 7.0-8.0 (m, 9H, Ar-H), 9.2 (s, 1H, NH). ¹³C NMR (100 MHz, DMSO-*d*₆) δ = 11.8, 19.2, 26.8, 28.9, 29.0, 29.5, 40.6, 50.8, 104.8, 110.6, 120.9, 123.8, 125.5, 125.8, 126.6, 128.8, 129.5, 129.2, 134.5, 136.2, 138.4, 148.0, 148.2, 151.6, 193.8. MS: M⁺1 = 398.

3,7,7-Trimethyl-4-phenyl-1-(*o*-tolyl)-6,7,8,9-tetrahydro-1H-pyrazolo[3,4-*b*]quinolin-5(4H)-one (4c)

Yield 85 %, m.p. 200-202 °C. ¹H NMR (400 MHz, DMSO-*d*₆) δ = 0.9 (s, 3H, CH₃), 1.0 (s, 3H, CH₃), 1.7 (s, 3H, CH₃), 1.9-2.2 (d, 4H, CH₂), 5.1 (s, 1H, CH), 7.0-8.0 (m, 9H, Ar-H), 9.3 (s, 1H, NH). ¹³C NMR (100 MHz, DMSO-*d*₆) δ = 11.9, 19.3, 26.9, 28.8, 31.2, 40.6, 50.8, 104.6, 110.0, 120.9, 123.5, 125.2, 125.9, 126.7, 128.9, 129.1, 129.3, 134.2, 136.3, 138.5, 145.3, 151.5, 194.2. MS: M⁺1 = 398.

1-(4-Methoxyphenyl)-3,7,7-trimethyl-4-phenyl-6,7,8,9-tetrahydro-1H-pyrazolo[3,4-*b*]quinolin-5(4H)-one (4d)

Yield 87 %, m.p. >220 °C. ¹H NMR (400 MHz, DMSO-*d*₆) δ = 0.9 (s, 3H, CH₃), 1.0 (s, 3H, CH₃), 1.8 (s, 3H, CH₃), 1.8-2.0 (d, 4H, CH₂), 3.6 (s, 3H, OCH₃), 5.0 (s, 1H, CH), 7.0-8.0 (m, 9H, Ar-H), 9.2 (s, 1H, NH). ¹³C NMR (100 MHz, DMSO-*d*₆) δ = 11.8, 26.8, 27.5, 28.7, 31.3, 34.2, 47.2, 50.1, 54.3, 104.5, 110.2, 113.1, 120.3, 123.2, 126.1, 126.8, 128.6, 129.5, 129.9, 130.2, 136.1, 138.2, 139.4, 145.2, 151.4, 156.6, 194.5. MS: M⁺1 = 414.

1-(2-Methoxyphenyl)-3,7,7-trimethyl-4-phenyl-6,7,8,9-tetrahydro-1H-pyrazolo[3,4-*b*]quinolin-5(4H)-one (4e)

Yield 90 %, m.p. >220 °C. ¹H NMR (400 MHz, DMSO-*d*₆) δ = 0.9 (s, 3H, CH₃), 1.0 (s, 3H, CH₃), 1.7 (s, 3H, CH₃), 1.8-2.0 (d, 4H, CH₂), 3.6 (s, 3H, OCH₃), 4.9 (s, 1H, CH), 7.0-8.0 (m, 9H, Ar-H), 9.3 (s, 1H, NH). ¹³C NMR (100 MHz, DMSO-*d*₆) δ = 11.9, 26.9, 27.7, 28.8, 31.8, 34.4, 47.6, 50.4, 54.8, 104.6, 110.0, 113.2, 120.5, 123.5, 126.2, 126.9, 128.7, 129.8, 129.9, 130.3, 136.2, 138.3, 139.5, 145.3, 151.5, 156.9, 194.2. MS: M⁺1 = 414.

1-(4-Chlorophenyl)-3,7,7-trimethyl-4-phenyl-6,7,8,9-tetrahydro-1H-pyrazolo[3,4-*b*]quinolin-5(4H)-one (4f)

Yield 90 %, m.p. 176-178 °C. ¹H NMR (400 MHz, DMSO-*d*₆) δ = 0.9 (s, 3H, CH₃), 1.0 (s, 3H, CH₃), 1.9 (s, 3H, CH₃), 2.1-2.3 (d, 4H, CH₂), 5.0 (s, 1H, CH), 6.5 (s, 1H, NH), 7.0-8.0 (m, 9H, Ar-H). ¹³C NMR (100 MHz, DMSO-*d*₆) δ = 12.1, 27.3, 28.9, 29.0, 32.5, 42.5, 50.8, 104.3, 111.9, 121.1, 124.5, 127.5, 129.3, 129.5, 129.9, 131.2, 135.6, 137.5, 144.1, 147.5, 148.9, 195.2. MS: M⁺ = 417, M+2 = 419.

1-(4-Fluorophenyl)-3,7,7-trimethyl-4-phenyl-6,7,8,9-tetrahydro-1H-pyrazolo[3,4-*b*]quinolin-5(4H)-one (4g)

Yield 89 %, m.p. 221-222 °C. ¹H NMR (400 MHz, DMSO-*d*₆) δ = 0.9 (s, 3H, CH₃), 1.0 (s, 3H, CH₃), 1.9 (s, 3H, CH₃), 2.1-2.3 (d, 4H, CH₂), 5.1 (s, 1H, CH), 6.6 (s, 1H, NH), 7.0-8.0 (m, 9H, Ar-H). ¹³C NMR (100 MHz, DMSO-*d*₆) δ = 12.1, 27.3, 28.9, 29.6, 32.5, 35.5, 42.2, 50.8, 104.5, 112.0, 121.9, 125.1, 126.9, 129.3, 129.8, 129.9, 135.6, 137.9, 142.3, 142.5, 148.9, 162.39, 195.2. MS: M⁺1 = 402.

1-(4-Ethylphenyl)-3,7,7-trimethyl-4-phenyl-6,7,8,9-tetrahydro-1H-pyrazolo[3,4-*b*]quinolin-5(4H)-one (4h)

Yield 90 %, m.p. >220 °C. ¹H NMR (400 MHz, DMSO-*d*₆) δ = 0.9 (s, 3H, CH₃), 1.0 (s, 3H, CH₃), 1.2 (t, 3H, CH₃),

1.9-2.2 (d, 4H, CH₂), 2.6 (q, 2H, CH₂), 5.0 (s, 1H, CH), 7.0-8.0 (m, 9H, Ar-H), 9.2 (s, 1H, NH). ¹³C NMR (100 MHz, DMSO-*d*₆) δ = 11.9, 15.0, 19.2, 26.8, 28.9, 31.1, 40.7, 50.9, 104.3, 110.1, 120.8, 123.4, 125.5, 125.8, 126.8, 128.8, 129.5, 129.9, 134.1, 136.2, 138.4, 145.2, 151.7, 194.1. MS: M⁺ = 412.

CONCLUSION

In summary, we have developed a simple and efficient green protocol for the synthesis of pyrazole-conjugated tetrahydroquinoline derivatives using 3-methyl-1-phenyl-1H-pyrazol-5-amine (1), 5,5-dimethylcyclohexane-1,3-dione (2) and benzaldehydes (3) as synthons by exploiting the eco-friendly characteristic of glycerol as green reaction medium. These pyrazole conjugates have exhibited potential cyto-toxic activity on breast cancer (MCF-7) and liver cancer (A549) cell lines. Further, molecular modelling studies gave an understanding about the target protein binding interactions with synthesized ligands. In addition, pharmacokinetic properties that were predicted using SwissADME tools gave details of the total polar surface area, BBB, ilogP and GI absorption. The information derived out of these would be helpful for the further structural optimization to get lead like molecules.

ACKNOWLEDGEMENT

The authors are very thankful to Excelra knowledge Solutions Private Limited, IDA Uppal, Hyderabad, Department of Bio-technology, Rayalaseema university, Kurnool, Andhra Pradesh and Department of Bio-Technology, S.V. University, Tirupati, Andhra Pradesh for permitting the research work and for constant encouragement.

REFERENCES

¹Karthikeyan, C., Malla, R., Ashby, C. R., Amawi, H., Abbott, K. L., Moore, J., Chen, J., Balch, C., Flannery, P. C., Trivedi, P., Lee, C., Faridi, J. S., Pondugula, S. R., Tiwari, A. K., Pyrimido[1",2":1,5]pyrazolo[3,4-*b*]quinolines: Novel compounds that reverse ABCG2-mediated resistance in cancer cells, *Cancer Lett.*, **2016**, *376*, 118–126. DOI: [10.1016/j.canlet.2016.03.030](https://doi.org/10.1016/j.canlet.2016.03.030)

²Karnakar, K., Narayana, S. M., Ramesh, K., Satish, G., Jagadeesh, B. N., Nageswar, Y. V. D., Polyethylene glycol (PEG-400): an efficient and recyclable reaction medium for the synthesis of pyrazolo[3,4-*b*]quinoline derivatives. *Tetrahedron Lett.*, **2012**, *53*, 2897-2903. <http://dx.doi.org/10.1016/j.tetlet.2012.03.135>

³Mohamed, L. W., Shaaban, M. A., Zaher, A. F., Elsahar, A. M., Synthesis of new pyrazoles and pyrazolo[3,4-*b*]pyridines as anti-inflammatory agents by inhibition of COX-2 enzyme, *Bioorg. Chem.*, **2019**, *83*, 47–54. DOI: [10.1016/j.bioorg.2018.10.014](https://doi.org/10.1016/j.bioorg.2018.10.014)

⁴Singh, S. K., Rebbi, P. G., Rao, K. S., Lohray, B. B., Misra, P., Rajjak, S. A., Rao, Y. K., Venkateswarlu, A., Polyethylene glycol (PEG-400): an efficient and recyclable reaction medium for the synthesis of pyrazolo[3,4-*b*]quinoline derivatives, *Bioorg. Med. Chem. Lett.*, **2004**, *14*, 499. <http://dx.doi.org/10.1016/j.tetlet.2012.03.135>

⁵Safaei-Ghomi, J., Sadeghzadeh, R., Shahbazi-Alavi, H., A pseudo six-component process for the synthesis of tetrahydrodipyrzolo pyridines using an ionic liquid immobilized on a FeNi₃ nanocatalyst, *RSC Adv.*, **2016**, *6*, 33676–33685. <https://doi.org/10.1039/C6RA02906J>

⁶Paul, S., Das, A. R., PEG-OSO₃H in aqueous reaction medium: synthesis of highly substituted structurally diversified coumarin and uracil fused spirooxindoles. *Tetrahedron Lett.*, **2013**, *54*, 1149–1154. <https://doi.org/10.1016/j.tetlet.2012.12.079>

⁷Bhattacharjee, D., Kshiar, B., Myrboh, B., L-Proline as an efficient enantioinduction organo-catalyst in the solvent-free synthesis of pyrazolo[3,4-*b*]quinoline derivatives via one-pot multi-component reaction. *RSC Adv.*, **2016**, *6*, 95944–95950. <https://doi.org/10.1039/C6RA22429F>

⁸Khurana, J. M., Chaudhary, A., Nand, B., Lumb, A., Aqua mediated indium(III) chloride catalyzed synthesis of fused pyrimidines and pyrazoles. *Tetrahedron Lett.*, **2012**, *53*, 3018–3022. <https://doi.org/10.1016/j.tetlet.2012.04.001>

⁹Ramesh, V., Purna, P. C. R., Ramachandran, D., Kalyan, A. C., One-pot syntheses of 2-(1H-benzo[d]oxazole-2-yl)-narylbenezamides by self-catalysis, *Eur. Chem. Bull.*, **2019**, *8*, 318-321. DOI: <http://dx.doi.org/10.17628/ecb.2019.8.318-321>

¹⁰Sheldon, R. A., Catalytic reactions in ionic liquids, *Chem. Commun.*, **2001**, 2399-2407. <https://doi.org/10.1039/B107270F>

¹³Toda, F., Tanaka, K., Solvent-free organic synthesis, *Chem. Rev.*, **2000**, *100*, 1025. <https://doi.org/10.1021/cr940089p>

¹⁴Luo, Z. Y., Zang, Q. S., Oderaotoshi, Y., Curran, D. P. Fluorous mixture synthesis: a fluororous-tagging strategy for the synthesis and separation of mixtures of organic compounds, *Science*, **2001**, *291*, 1766. DOI: [10.1126/science.1057567](https://doi.org/10.1126/science.1057567)

¹⁵Temple, C., Rose, J. D., Comber, R. N., Renner, G. A. Synthesis of potential anticancer agents: imidazo[4,5-*c*]pyridines and imidazo[4,5-*b*]pyridines, *J. Med. Chem.*, **1987**, *30*, 1746. <https://doi.org/10.1021/jm00393a011>

¹⁶Kehinde, I., Ramharack, P., Nlooto, M. and Gordon, M., The pharmacokinetic properties of HIV-1 protease inhibitors: A computational perspective on herbal phytochemicals, *Heliyon*, **2019**, *5*, 02565. DOI: [10.1016/j.heliyon.2019.e02565](https://doi.org/10.1016/j.heliyon.2019.e02565)

¹⁷Daina, A., Michielin, O. Zoete, V., SwissADME: a free web tool to evaluate pharmacokinetics, drug-likeness and medicinal chemistry friendliness of small molecules, *Sci. rep.*, **2017**, *7*, 42717. DOI: [10.1038/srep42717](https://doi.org/10.1038/srep42717)

¹⁸Ji, D., Xu, M., Udenigwe, C.C., Agyei, D., Physicochemical characterisation, molecular docking, and drug-likeness evaluation of hypotensive peptides encrypted in flaxseed proteome, *Curr. Res. Food Sci.*, **2020**, *3*, 41-50. <https://doi.org/10.1016/j.crf.2020.03.001>

¹⁹Mosmann T., Rapid colorimetric assay for cellular growth and survival: application to proliferation and cytotoxicity assays, *J. Immunol. Methods*, **1983**, *65*, 55-63. DOI: [10.1016/0022-1759\(83\)90303-4](https://doi.org/10.1016/0022-1759(83)90303-4).

²⁰Ghanbari-Ardestani, S., Khojasteh-Band, S., Zaboli, M., Hassani, Z., Mortezaei, M., Mahani, M., Torkezadeh-Mahani, M., The effect of different percentages of triethanolammonium butyrate ionic liquid on the structure and activity of urate oxidase: Molecular docking, molecular dynamics simulation, and experimental study. *J. Mol. Liq.*, **2019**, *292*, 111318. DOI: [10.1016/j.molliq.2019.111318](https://doi.org/10.1016/j.molliq.2019.111318)

²¹Wallace, A. C., Laskowski, R. A., Thornton, J. M., LIGPLOT: a program to generate schematic diagrams of protein-ligand interactions, *Protein Eng. Des. Sel.*, **1995**, *8*, 127-134. DOI: [10.1093/protein/8.2.127](https://doi.org/10.1093/protein/8.2.127)

Received: 17.04.2020.

Accepted: 19.06.2020.



CAROB (*CERATONIA SILIQUA*): SUPER FOOD AND MEDICINE. LITERATURE UPDATE

Abdullatif Azab^{[a]*}

Keywords: Carob; antioxidant; cultivation; cocoa substitute; male fertility; gluten-free; molasses, nutrition.

Carob (*Ceratonia siliqua*) is one of the important nutritional and medicinal trees of the Middle East and Mediterranean basin, and in recent decades, it has been grown and cultivated in many other regions in the world. Realization and awareness to its unique nutritional and medicinal properties and biological activities are rising rapidly. A great effort of research has been invested and published since our comprehensive review article was published here, in this journal, in 2017. Most recent publications focus on nutrition and efforts to utilize Carob products for numerous food purposes, but medicinal activities of this tree are still drawing major attention, due to their high potential. In this review article, we are presenting a literature update of published research since late 2017. The main objective of this review is to highlight the nutritional applications of Carob products, which many industrial companies in the world, are trying now to convert to commercial food products.

*Corresponding Author

Fax: +972-4-6205906

Phone: +972-50-5650025

E-Mail: eastern.plants@gmail.com

[a] Eastern Plants Research Institute, Box 868, Arara, Israel
30026

INTRODUCTION

Carob (*Ceratonia siliqua*) is a tree that was domesticated in the Middle-East in ancient times, but it is currently cultivated in many other regions in the world.¹ Since the publication of our comprehensive review about this tree in 2017,² the average number of publication per a year is rising rapidly.

According to our literature study, it is clear that until 2017, most publications focused on studying medicinal activities of various products of this plant, such as extracts and oils. In recent years, nutritional research is gaining larger value and importance, yet, medicinal research is still interesting and exploring new activities. Consequently, in this review we will present in wider view the nutritional aspects of Carob research, and in the discussion section, we will relate to some notable cultivation efforts of this tree.

In the last three years, few important review articles were published about medicinal and nutritional properties of Carob. A. Loullis and E. Pinakoulaki discussed carob pod powder as a potential cocoa substitute.³ The key importance of this review is the presentation and comparison of active compounds in both foods, mainly phenolics, such as flavonoids and anthocyanins. I. Lakkab and her colleagues published a medium size excellent article about the neuroprotective activities of Carob.⁴ They presented the biological relation between oxidative stress and neurodegenerative diseases, medicinal activities of Carob focusing on antioxidant activity, general chemical composition and suggestions for future research. Polysaccharides content of various parts of Carob tree were clearly presented by B-J. Zhu and his colleagues.⁵ They

showed clear structures and discussed the current and possible applications of Carob nutrients. A small size, yet summarily written review was published by K. Ghedira and P. Goetz.⁶ It briefly presented botany, ecology, selected medicinal activities and some active compounds. Finally, a very important review was published by J. I. Lopez-Sanchez and his colleagues, and it discussed the importance of D-pinitol (Figure 1), an active polyhydroxy, cyclic alcohol found in Carob pods.⁷ Authors presented the structure, physical properties, natural sources, synthesis and many health promoting effects of this natural product. In addition, many synthetic derivatives are introduced along with their biological activities.

We present here some of these derivatives in Figure 1. Based on their presentation of D-pinitol, authors named this compound "super food".

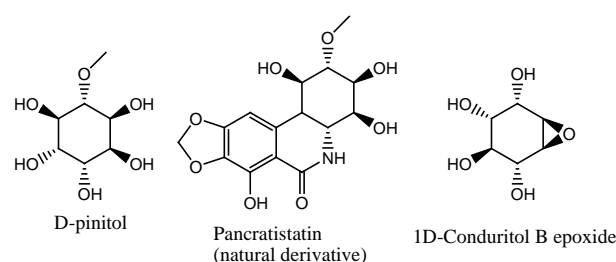


Figure 1. D-pinitol and some of its selected derivatives (ref. 7).

MEDICINAL, BIOLOGICAL AND OTHER ACTIVITIES

Research of classical medicinal and related properties is ongoing, but in the last three years, there has been a notable increase in the studies of Carob as food and nutrition source. It is important to emphasize that classical research is still exploring very new activities that were not reported in our previous publication, such as treatment of male infertility. A summary of these properties is presented in Table 1.

Table 1. Medicinal, nutritional and other properties of *C. siliqua*.

Property/Activity	Methods/Results/Reference
Antibacterial, antifungal and related activities	Hydrodistillation was used to extract essential oil (EO) from dried pods. EO was active against several bacteria species. ⁸ Leaves and green pods were extracted with ethanol and extract was found active against <i>F. oxysproum</i> and <i>M. fructigena</i> . ⁹ Leaves were extracted with water and ethanol, and both extracts were active against several species of fish infecting bacteria. Other properties were also reported but not detailed. ¹⁰
Antidiabetic and related activities	Methanolic extract of dry, unripe pods was active against STZ-nicotinamide-induced hyperglycemia in rats. ¹¹ Carob honey was extracted with water and ethyl acetate. Both extracts showed hypoglycemic activity in STZ-induced diabetes in rats. ¹²
Antidiarrheal, antiemetic	Dry unripe pods were extracted with 70% aqueous methanol, and extract was fractionized with water and dichloromethane. Both fractions were analyzed for general chemical composition and were found active antidiarrheal and antiemetic in rat model. ¹³
Antioxidant, and related activities	EO was extracted from dried pods and was tested for antioxidant activity (DPPH). ⁸ Methanolic extract of dry, unripe pods was active antioxidant (DPPH, FRAP). ¹¹ Carob honey was extracted with water and ethyl acetate and both extracts had antioxidant activity (ABTS). ¹² Dry ripe pods were extracted with methanol and extract had activity against lipid peroxidation in rat model. ¹⁴ General chemical composition and antioxidant activity (DPPH) were determined for honeys. ¹⁵ Aqueous extracts was prepared from the ripe pods of two "Carob" trees: <i>Ceratonia siliqua</i> and <i>Prosopis alba</i> . Both extracts were analyzed for general chemical composition and their antioxidant activity (DPPH) was compared: <i>C. siliqua</i> extract had higher activity. ^{16a} Aqueous extracts of pods in different ripening stages were prepared and analyzed for general chemical composition and tested for antioxidant activity (DPPH). ¹⁷ Dry ripe pods were roasted with hot air and microwave radiation, then extracted with water. The extract had high antioxidant activity (DPPH), high sugar and D-pinitol contents, and authors reports that there was 50 % energy saving in this roasting process compared with regular roasting. ¹⁸ Seeds were extracted

Cardioprotective, metabolic syndrome	with several solvents and analyzed for fatty acids, lipidic compounds, amino acids, phenolics, monosaccharides, all in details. Some activities of galactomannan fractions were tested. Antioxidant activity was determined by DPPH method. ¹⁹ Commercial aqueous extracts of pods and seeds, along with Carob fructooligosaccharides were supplemented to mice. This resulted in cardioprotective activity and amelioration of metabolic syndrome in mice. Antioxidant capacity of this mixture was determined (ABTS). ²⁰ This comprehensive research used Carob industry by-products that were extracted with methanol and 50% aqueous methanol. Extracts were analyzed for general chemical composition, total phenolic content, and tested for antioxidant activity (4 methods), ACE inhibition, anti-inflammatory activity (3 tests, triglyceride content (metabolic syndrome)). ²¹
Fertility (male)	Busulfan-induced infertility in mice was treated with Carob aqueous extract (plant part/s not reported). As a result, sperm quality improved, biochemical parameters related to fertility were also improved, including testosterone. ²² Rabbits were treated with seeds aqueous extract, and there were positive changes in concentrations of sperm, plasma and testosterone. ²³ Infertile men were treated with 1500 mg capsules of mature pods aqueous extract, resulting improvement in sperm count and quality. ²⁴ Leaves and fruits were extracted with water and extract was administered to normozoospermic aged men, resulting improvement of sperm and chromatin. ²⁵ Dried pods aqueous extract was injected to mice. The dose of 200 mg kg ⁻¹ of body weight, was most efficient in increasing testicular index, sperm parameters and decreased the level of oxidative stress. ²⁶ Infertile men in ages 25-40 years were treated with a combination of Carob syrup and vitamin E. As a result, sperm and sex hormones increased. ²⁷ Dried pods were extracted with 96% aqueous ethanol. The extract was supplemented to mice with Pb (lead) reproductive toxicity, resulting improvement of sperm, sex hormones and other biochemical fertility parameters. ²⁸
Hepatoprotective	Carob honey was extracted with water and ethyl acetate. Both extracts showed hepatoprotective activity. ¹² Aqueous

Neuroprotective and brain related activities	<p>extract of ripe, dry pods was prepared and administered to rats that were exposed daily to tobacco waterpipe smoke. Positive results were recorded in amelioration of lung injuries.²⁹</p> <p>Dry unripe pods were extracted with 70 % aqueous methanol, and extract was fractionized with water and dichloromethane. Both fractions were antispasmodic in rat model.¹³ Aqueous extract of ripe, dry pods was prepared and administered to rats that were exposed daily to tobacco waterpipe smoke. Positive results were recorded in amelioration of brain injuries.²⁹ Rats were fed with plus-maze resulting emotional disorders and estrogen deficiency. They were treated with pods aqueous extract that altered these diet effects.³⁰ Parkinson disease model was induced in Zebrafish by neurotoxic 6-hydroxydopamine. After treatment with leaves aqueous extract, antioxidant and anti-AChE activity was recorded, resulting improvement of cognitive function.³¹</p>	strong antioxidant and cytotoxic activities. ⁴² Leaves aqueous extract was reacted with $Zn(CH_3COO)_2$ to prepare ZnO-NPs. These NPs had strong cytotoxic activity against human breast cancer cells. ⁴³
Skin Protection	<p>Aqueous extract of fruits and leaves had notable activity of skin regeneration and wound healing.³² A follow-up study by the same research group, but with clinical trials.³³</p>	<p>Chemical composition</p> <p>Proteins, amino acids and sugar contents were determined in pods at different harvesting stages.⁴⁴ Leaves were extracted with pressurized hot water and fractionized with various solvents, resulting isolation and characterization of a new natural product, that researchers named siliquapyranone (Figure 2, below table, after note a).⁴⁵ Solid-phase micro-extraction / gas chromatography-mass spectrometry (SPME/GC-MS) analyses of flowers and fruits were performed, and detailed composition of volatile compounds is reported.⁴⁶</p>
Chemical applications, processing and extraction	<p>Solid Carob waste from food industry was used for production of bio-hydrogen. The process was studied under various reaction conditions: pH, catalysis, nitrogen environment, water supply; and yield was compared to glucose a control substrate.³⁴ Pods were extracted with water and bacteria fermented. Several ionic liquids were tested for extraction of dry ethanol instead of ethylene glycol.³⁵ Microwave assisted extraction of phenolics afforded higher yields than non-radiated extraction.³⁶ Thin layer pulp drying conditions were studied and optimized.³⁷ Spray drying tested and proved successful in improving the quality and yields for drying of Carob juice.³⁸ Various roasting conditions were tested in order to achieve optimal properties, such as sensory, antioxidant, aromas and physiochemical.³⁹ Pods were extracted for sugar content, using the mathematical Taguchi method to design the extraction. Practically, pods were extracted four times successively.⁴⁰ Powder of dry, ripe pods was found successful absorbent of dye pollution (methylene blue).⁴¹ Leaves aqueous extract was used to prepare CeO_2 nanoparticles (NPs) by reaction with $Ce(NO_3)_3 \cdot 6H_2O$. These NPs had</p>	<p>Animal food</p> <p>Syrup was supplemented to Tilapia Fish (<i>O. mossambicus</i>) in different concentrations. It was found that the optimal was 1.25%, which notably decreased serum glucose, triglyceride, cholesterol levels, it significantly increased the phagocytic activity, phagocytic index, respiratory burst and potential killing activity. No toxicity was recorded.⁴⁷ Pods were supplied as food to sheep resulting high nutritional values.⁴⁸</p>
		<p>Human food and nutrition</p> <p>Candies were prepared from pod powder as wheat flour substitute, dates and olive fruits. Physical and chemical parameters (nutritional values, antioxidant capacity, FRAP) were reported.⁴⁹ Near Infrared spectroscopy technique was developed to detect Carob flour in cocoa powder.⁵⁰ Cakes were prepared from pod powder as cocoa powder partial substitute. Physical and chemical parameters (nutritional values, antioxidant capacity, ABTS, DPPH) were reported.⁵¹ Pod powder was used to replace wheat flour (40 or 60%) in Cupcakes, and physical and chemical properties were improved, especially fat and sugar replacement.⁵² Soft drink was prepared from pods pulp and it had high physical and chemical qualities.⁵³ Analysis of seed peel revealed 90% content of dietary fibers.⁵⁴ Rice flour and pods powder were used to prepare gluten-free cakes, and results of various tests are reported.⁵⁵ Pods powder was used as wheat flour substitute in muffins and positive physicochemical (weight loss, antioxidant, DPPH, ABTS) results were recorded.⁵⁶ Bean molasses was used to produce low-calorie ice cream, with</p>

high nutritional values.⁵⁷ Pods molasses were mixed with sesame paste, resulting notable physical changes (color, viscosity) as well as rise in nutritional value (mainly proteins).⁵⁸ A follow-up study to the previous one, where pods molasses were analyzed for physiochemical characteristics.⁵⁹ Detailed analysis of five samples of molasses to determine the content of 18 nutritionally important phenolic compounds.⁶⁰ A comprehensive study that analyzed different parts of Carob tree (excluding roots) for sugars, proteins, enzyme inhibition and other general chemical properties.⁶¹ High quality and pioneering study that analyzed 20 commercial Carob food products used in Cyprus. Detailed analyses of major nutritional parameters are presented.⁶² Pastry filling was prepared with pods flour and bean gum, and the rheological (texture, flow) were notably improved. Mathematical model was used for the products design.⁶³ Adding Carob syrup and/or flour to sponge cakes increased their protein, fiber and carbohydrate contents.⁶⁴ Polyphenol-rich pod extract was supplemented to Taekwondo athletes for 6 weeks. As a result, reduction of body weight and improvement of aerobic performance were recorded.⁶⁵

(a) Authors of ref. 16 consider *Prosopis alba* “White Carob” because in South America its common name is Algarrobo Blanco, which stands for “White Carob” in Spanish. We have related to the issue of common names in previous publications, and to the fact that they can be misleading. *Ceratonia* and *Prosopis* genera belong to the same family, *Fabaceae*, but they are not the same genus. *Prosopis* is not Carob.

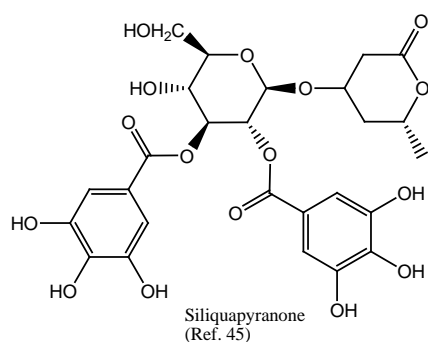


Figure 2. Structure of Siliquapyranone (ref. 45).

DISCUSSION

In the last two decades, the interest in Carob is rising rapidly, and according to research publications about this tree, it seems that it will have great importance in future human nutrition, economy and medicine.

Numerous studies were published about the optimal methods of cultivating this tree. In terms of environmental efficiency, P. J. Corriera and his colleagues recommended growing Carob in mixed orchards with another classical Middle-eastern crops, such as Fig, Almond and Olive trees.⁶⁶ A. Gugliuzzo and his colleagues discuss the damage that natural enemies of Carob can do to this tree, especially insects (mainly Carob moth, *Ectomyeloisceratoniae*) and fungi.¹ And in order to make the best selection of wild varieties for domestic cultivation, N. Korkmaz and her colleagues discuss the various parameters that affect tree morphology, fruiting yield, quality and composition, in wild-grown trees.⁶⁷ Along with these studies, many have investigated the effect of growth stressors such as dry farming,⁶⁸ or growth promoters like ultrasonic radiation,⁶⁹ iron and other nutrients⁷⁰ and cytokinins.⁷¹

However, it seems that the hottest medicinal research of Carob in the next few years will be treatment of male infertility.²²⁻²⁸ To the best of our knowledge, this activity in regard of Carob tree, is not known in Middle-eastern medicines, contrary to female infertility, which is treated with pollen grains of this tree.⁷² Modern review articles did not recognize yet this very important medicinal activity of Carob,⁷³ but since most studies agree that oxidative stress has major role in inducing male infertility,⁷⁴ Carob has great potential of treating this global health concern.

CONCLUSIONS

- (1) Medicinal properties of Carob have to be additionally studied, especially treatment of male infertility.
- (2) The nutritional and economic potential of Carob are huge. In order to maximize them, more research should be invested in Carob's health and nutrition benefits.

REFERENCES

- ¹Gugliuzzo, A., Mazzeo, G., Mansour, R., Garzia, G. T., Carob pests in the Mediterranean region: bio-ecology, natural enemies and management options, *Phytoparasitica*, **2019**, *47*, 605–628. <https://doi.org/10.1007/s12600-019-00766-7>
- ²Azab, A., Carob (*Ceratonia siliqua*): Health, Medicine and Chemistry, *Eur. Chem. Bull.*, **2017**, *6*, 456-469. DOI: 10.17628/ecb.2017.6.456-469
- ³Loullis, A., Pinakoulaki, E., Carob as cocoa substitute: a review on composition, health benefits and food applications, *Eur. Food Res. Technol.*, **2018**, *244*, 959–977. <https://doi.org/10.1007/s00217-017-3018-8>
- ⁴Lakkab, I., El Hajaji, H., Lachkar, N., El Bali, B., Lachkar, M., Ciobica, A., Phytochemistry, bioactivity: suggestion of *Ceratonia siliqua* L. as neurodegenerative disease Therapy, *J. Complement. Integr. Med.*, **2018**, *15*, Article 20180013. DOI: 10.1515/jcim-2018-0013
- ⁵Zhu, B-J., Zayed, M. Z., Zhu, H-X., Zhao, J., Li, S-P., Functional polysaccharides of Carob fruit: a review, *Chin. Med.*, **2019**, *14*, Article 40. <https://doi.org/10.1186/s13020-019-0261-x>
- ⁶Ghedira, K., Goetz, P., Caroubier : *Ceratonia siliqua* (L.) (Fabaceae), *Phytotherapie*, **2019**, *17*, 286-290. DOI: 10.3166/phyto-2019-0197

- ⁷Lopez-Sanchez, J. I., Moreno, D. A., Garcia-Viguera, C., D-pinitol, a highly valuable product from carob pods: Health-promoting effects and metabolic pathways of this natural super-food ingredient and its derivatives, *AIMS Agric. Food*, **2018**, 3, 41-63. DOI: 10.3934/agrfood.2018.1.41
- ⁸Ouis, N., Hariri, A., Antioxidant and antibacterial activities of the essential oils of *Ceratonia siliqua*, *Banat's J. Biotechnol.*, **2018**, 9, 13-23. DOI: 10.7904/2068-4738-IX(17)-13
- ⁹Yavuz, A., Onaran, A., Yanar, Y., Antifungal Activity of Leaf Extract of *Ceratonia Siliqua* L. Plant Against Plant Pathogenic Fungi, *Int. J. Agric. Nat. Sci.*, **2018**, 1, 36-38. <http://ijans.org/index.php/ijans/article/view/413/401>
- ¹⁰Ben Othmen, K., Elfalleh, W., Beltran, J. M., Esteban, M. A., Haddad, M., An invitro study of the effect of carob (*Ceratonia siliqua* L.) leaf extracts on gilthead seabream (*Sparus aurata* L.) leucocyte activities, Antioxidant, cytotoxic and bactericidal properties, *Fish Shellfish Immunol.*, **2020**, 99, 35-43. DOI:10.1016/j.fsi.2020.02.005
- ¹¹Qasem, M. A., Noordin, M. I., Arya, A., Alsalahi, A., Jayash, S. N., Evaluation of the glycemic effect of *Ceratonia siliqua* pods (Carob) on a streptozotocin-nicotinamide induced diabetic rat model, *Peer J.*, **2018**, 6, Article e4788. DOI: 10.7717/peerj.4788
- ¹²El-Haskoury, R., Al-Waili, N., El-Hilaly, J., Al-Waili, W., Lyoussi, B., Antioxidant, hypoglycemic, and hepatoprotective effect of aqueous and ethyl acetate extract of Carob honey in streptozotocin-induced diabetic rats, *Vet. World*, **2019**, 12, 1916-1923. www.doi.org/10.14202/vetworld.2019.1916-1923
- ¹³Hamid, I., Janbaz, K. H., Ethnopharmacological basis for antispasmodic, antidiarrheal and antiemetic activities of *Ceratonia siliqua* pods, *Bangladesh J. Pharmacol.*, **2017**, 12, 384-392. DOI: 10.3329/bjp.v12i4.33218
- ¹⁴Al-Seeni, M. N., El Rabey, H. A., Al-Ghamdi, H., Al-Sieni, A. I., Sakran, M. I., Mohammed, G. M., Assessment of the antioxidant activity of parsley and carob in hypercholesterolemic male rats, *Biomed. Res.*, **2018**, 29, 3370-3377. <https://www.researchgate.net/publication/328381662>
- ¹⁵El-Haskoury, R., Kriaa, W., Lyoussi, B., Makni, M., *Ceratonia siliqua* honeys from Morocco: Physicochemical properties, mineral contents, and antioxidant activities, *J. Food Drug Anal.*, **2018**, 26, 67-73. <http://dx.doi.org/10.1016/j.jfda.2016.11.016>
- ¹⁶Carbas, B., Salinas, M. V., Serrano, C., Passarinho, J. A., Puppo, M. C., Ricardo, C. P., Brites, C., Chemical composition and antioxidant activity of commercial flours from *Ceratonia siliqua* and *Prosopis* spp., *J. Food Meas. Charact.*, **2019**, 13, 305-311. <https://doi.org/10.1007/s11694-018-9945-7>
- ¹⁷Ben Othmen, K., Elfalleh, W., Lachiheb, B., Haddad, M., Evolution of phytochemical and antioxidant activity of Tunisian carob (*Ceratonia siliqua* L.) pods during maturation, *EuroBiotech J.*, **2019**, 3, 135-142. DOI: 10.2478/ebtj-2019-0016
- ¹⁸Gunel, Z., Torun, M., Sahin-Nadeem, H., Sugar, D-pinitol, volatile composition, and antioxidant activity of carob powder roasted by microwave, hot air, and combined microwave/hot air, *J. Food Process. Preserv.*, **2020**, 44, Article e14371. <https://doi.org/10.1111/jfpp.14371>
- ¹⁹Fidan, H., Stankov, S., Petkova, N., Petkova, Z., Iliev, A., Stoyanova, M., Ivanova, T., Zhelyazkov, N., Ibrahim, S., Stoyanova, A., Ercisli, S., Evaluation of chemical composition, antioxidant potential and functional properties of carob (*Ceratonia siliqua* L.) seeds, *J. Food Sci. Technol.*, **2020**, 57, 1-10. <https://doi.org/10.1007/s13197-020-04274-z>
- ²⁰Fuente-Fernández, M., Gonzalez-Hedstrom, D., Amor, S., Tejera-Munoz, A., Fernandez, N., Monge, L., Almodovar, P., Andres-Delgado, L., Santamaria, L., Prodanov, M., Inarejos-Garcia, A. M., Garcia-Villalon, L. A., Granado, M., Supplementation with a Carob (*Ceratonia siliqua* L.) Fruit Extract Attenuates the Cardiometabolic Alterations Associated with Metabolic Syndrome in Mice, *Antioxidants*, **2020**, 9, 339-363. DOI:10.3390/antiox9040339
- ²¹Rico, D., Martin-Diana, A. B., Martinez-Villaluenga, C., Aguirre, L., Silvan, J. M., Duenas, M., De Luis, D. A., Lasa, A., In vitro approach for evaluation of carob byproducts as source bioactive ingredients with potential to attenuate metabolic syndrome (MetS), *Heliyon*, **2019**, 5, Article e01175. DOI: 10.1016/j.heliyon.2019
- ²²Vafaei, A., Mohammadi, S., Fazel, A., oukhtanloo, M., Pour, A.M., Beheshti, F., Effects of Carob (*Ceratonia siliqua*) on Sperm Quality, Testicular Structure, Testosterone Level and Oxidative Stress in Busulfan-Induced Infertile Mice, *Pharmaceut. Sci.*, **2018**, 24, 104-111. DOI: 10.15171/PS.2018.16
- ²³Ata, A., Yildiz-Gulay, O., Gungor, S., Balic, A., Gulay, M. S., The Effect of Carob (*Ceratonia siliqua*) Bean Extract on Male New Zealand White Rabbit Semen, *World Rabbit Sci.*, **2018**, 26, 209-215. DOI:10.4995/wrs.2018.10154
- ²⁴Mahdiani, E., Haghghighian, H. K., Javadi, M., Karami, A. A., Kavianpour, M., Effect of Carob (*Ceratonia siliqua* L.) oral supplementation on changes of semen parameters, oxidative stress, inflammatory biomarkers and reproductive hormones in infertile men, *Sci. J. Kurdistan Univ. Med Sci.*, **2018**, 95, 56-66. <https://www.researchgate.net/publication/328393315>
- ²⁵Faramarzi, A., Aghaz, F., Bakhtiari, M., Khazaei, M., In vitro application of *Ceratonia siliqua* improved sperm parameters and chromatin quality after vitrification in normozoospermic aged men, *Middle East Fertil. Soc. J.*, **2019**, 24, Article 6. <https://doi.org/10.1186/s43043-019-0007-9>
- ²⁶Sadat, S. S., Mohammadi, S., Sazegar, G., Fazel, A., Ebrahimzadeh, A., Mobarhan, M. G., Beheshti, F., Attari, S. S., ShimaTavallaei, S., Effects of Carob Fruit Extract on Spermatogenesis, Antioxidant Status, and Apoptosis in Adult Male Mice, *Pharmaceut. Sci.*, **2019**, 25, 184-189. DOI: 10.15171/PS.2019.28
- ²⁷Aghajani, M. M., Gorji, N., Mirabi, P., Mojab, F., Effect of *Ceratonia siliqua* (Carob) syrup and vitamin E on sperm parameters, oxidative stress index and sex hormones in infertile men: Protocol for a randomized controlled trial, *Caspian J. Intern. Med.*, **2019**, 10, 452-457. DOI: 10.22088/cjim.10.4.452
- ²⁸Soleimanzadeh, A., Kian, M., Moradi, S., Mahmoudi, S., Carob (*Ceratonia siliqua* L.) fruit hydro-alcoholic extract alleviates reproductive toxicity of lead in male mice: evidence on sperm parameters, sex hormones, oxidative stress biomarkers and expression of *Nrf2* and *iNOS*, *Avicenna J. Phytomed.*, **2020**, 10, 35-49. <https://www.ncbi.nlm.nih.gov/pmc/articles/PMC6941692/>
- ²⁹Abdel-Rahman, M., Bauomy, A. A., Salem, F-E., Khalifa, M. A., Carob extract attenuates brain and lung injury in rats exposed to waterpipe smoke, *Egypt. J. Basic Appl. Sci.*, **2018**, 5, 31-40. DOI: 10.1016/j.ejbas.2018.01.004
- ³⁰Ammari, M., Othman, H., Rtibi, K., Sakly, M., Abdelmelek, H., The Effects of Carob (*Ceratonia siliqua* L.) on Emotional Behavior Impairment and Metabolic Disorders Induced by Estrogen Deficiency in Rats, *J. Med. Food*, **2020**, Ahead of print. DOI: 10.1089/jmf.2019.0187
- ³¹Abidar, S., Boiangiu, R. S., Dumitru, G., Todirascu-Ciornea, E., Amakran, A., Cioanca, O., Hritcu, L., Nhiri, M., The Aqueous Extract from *Ceratonia siliqua* Leaves Protects against 6-Hydroxydopamine in Zebrafish: Understanding the Underlying Mechanism, *Antioxidants*, **2020**, 9, 304-334. DOI:10.3390/antiox9040304
- ³²Hare, M., Flagler, M., Henry, J., Impact of carob extract on epidermal regeneration processes and cellular behavior invitro, *J. Am. Acad. Dermatol.*, **2017**, 76, Article AB403. <https://doi.org/10.1016/j.jaad.2017.06.059>
- ³³Flagler, M., Osborne, R., Mullins, L., d'Alessandro, B., Tamura, M., Ehrman, M., Dowdy, A., Ellis, K., In vivo efficacy of a cosmetic skin care product containing carob extract, *J. Am. Acad. Dermatol.*, **2018**, 79, Article AB165. <https://doi.org/10.1016/j.jaad.2018.05.675>

- ³⁴Bahry, H., Abdallah, R., Chezeau, B., Pons, A., Taha, S., Vial, C., Biohydrogen production from carob waste of the Lebanese industry by dark fermentation, *Biofuels*, **2019**, *10*, 1-11. DOI: 10.1080/17597269.2019.1669862
- ³⁵Sanchez-Segado, S., Salar-García, M. J., Ortiz-Martinez, V. M., Rios, A. P., Hernandez-Fernandez, F. J., Lozano-Blanco, L. J., Evaluation of Ionic Liquids as In Situ Extraction Agents during the Alcoholic Fermentation of Carob Pod Extracts, *Fermentation*, **2019**, *5*, 90-101. DOI:10.3390/fermentation5040090
- ³⁶Huma, Z-E., Jayasena, B., Nasar-Abbas, S. M., Imran, M., Khan, M. K., Process optimization of polyphenol extraction from carob (*Ceratonia siliqua*) kibbles using microwave-assisted technique, *J Food Process. Preserv.*, **2018**, *42*, Article e13450. <https://doi.org/10.1111/jfpp.13450>
- ³⁷Tagnamas, Z., Bahammou, Y., Kouhila, M., Lamharrar, A., Idlimam, A., Thin layer solar drying of Moroccan carob pulp (*Ceratonia Siliqua* L.), *IOP Conf. Ser.: Earth Environ. Sci.*, **2018**, *161*, Article 012007. DOI:10.1088/1755-1315/161/1/012007
- ³⁸Ali, H., Al-khalifa, A. R., Aboelsood, W., Bareh, G., Farouk, A., Influence of spray-drying on improving the quality of dried carob juice, *Qual. Assur. Saf. Crop. Food.*, **2019**, *11*, 391-399. DOI: 10.3920/QAS2018.1524
- ³⁹Boublenza, I., Lazouni, H. A., Ghaffari, L., Ruiz, K., Fabiano-Tixier, A-S., Chemat, F., Influence of Roasting on Sensory, Antioxidant, Aromas, and Physicochemical Properties of Carob Pod Powder (*Ceratonia siliqua* L.), *J. Food Qual.*, **2017**, Article 4193672. <https://doi.org/10.1155/2017/4193672>
- ⁴⁰Durmaz, U., Ozel, M. B., An Experimental Study on Extraction of Sugar from Carob Using with Taguchi Method, *Sakarya Univ. J. Sci.*, **2019**, *23*, 916-923. DOI:10.16984/saufenbilder.541940
- ⁴¹Gezer, B., Adsorption Capacity for the Removal of Organic Dye Pollutants from Wastewater Using Carob Powder, *Int. J. Agric. Forest. Life Sci.*, **2018**, *2*, 1-14. <http://www.ijafsls.org/en/issue/37327/431667>
- ⁴²Javadi, F., Yazdi, M. E., Baghani, M., Es-haghi, A., Biosynthesis, characterization of cerium oxide nanoparticles using *Ceratonia siliqua* and evaluation of antioxidant and cytotoxicity activities, *Mater. Res. Express*, **2019**, *6*, Article 065408. <https://doi.org/10.1088/2053-1591/ab08ff>
- ⁴³Raeisalsadati, A. S., Pouresmaeil, V., Neamati, A., Evaluation of the cytotoxic effect of greens synthesized zinc oxide nanoparticles with *Ceratonia siliqua* extract on the breast cancer cell line (MDA-MB231) and its antiangiogenic effects, *J. Neyshabur Univ. Med. Sci.*, **2019**, *7*, 58-72. <http://journal.nums.ac.ir/article-1-561-en.pdf>
- ⁴⁴Simsek, S., Ozcan, M. M., Al Juhaimi, F., ElBabiker, E., Ghafoor, K., Amino Acid and Sugar Contents of Wild and Cultivated Carob (*Ceratonia siliqua*) Pods Collected in Different Harvest Periods, *Chem. Nat. Compd.*, **2017**, *53*, 1008-1009. <https://doi.org/10.1007/s10600-017-2187-9>
- ⁴⁵Deans, B. J., Skierka, B. E., Karagiannakis, B. W., Vuong, D., Lacey, E., Smith, J. A., Bissember, A. C., Siliquapyranone: A Tannic Acid Tetrahydropyran-2-one Isolated from the Leaves of Carob (*Ceratonia siliqua*) by Pressurised Hot Water Extraction. *Aust. J. Chem.*, **2018**, *71*, 702-707. <https://doi.org/10.1071/CH18265>
- ⁴⁶Krokou, A., Stylianou, M., Agapiou, A., Assessing the volatile profile of carob tree (*Ceratonia siliqua* L.), *Environ. Sci. Pollut. Res.*, **2019**, *26*, 35365-35374. <https://doi.org/10.1007/s11356-019-04664-7>
- ⁴⁷Yilmaz, S., Sebahattin E. S., Celik, E.S., The Effect of Dietary Carob (*Ceratonia siliqua*) Syrup on Growth Performance, Haematological, Serum Biochemical and Immunological Parameters in Tilapia (*Oreochromis mossambicus*), *Turk. J. Agric. Food Sci. Technol.*, **2018**, *6*, 1820-1826. <https://doi.org/10.24925/turjaf.v6i12.1820-1826.2184>
- ⁴⁸Medjekal, S., Bodas, R., Bousseboua, H., Lopez, S., Evaluation of Carob (*Ceratonia siliqua*) and Honey Locust (*Gleditsia triacanthos*) Pods as a Feed for Sheep, *Iran. J. Appl. Anim. Sci.*, **2018**, *8*, 247-256. <https://www.researchgate.net/publication/325539371>
- ⁴⁹Radia, A., Boukhiar, A., Kechadi, K., Benamara, S., Preparation of a Natural Candy from Date (*Phoenix dactylifera* L.), Olive (*Olea europaea* L.), and Carob (*Ceratonia siliqua* L.) Fruits, *J. Food Qual.*, **2018**, Article 9565931. DOI: 10.1155/2018/9565931
- ⁵⁰Quelal-Vasconez, M. A., Perez-Esteve, E., Arnau-Bonachera, A., Barat, J. M., Talens, P., Rapid fraud detection of cocoa powder with carob flour using near infrared spectroscopy, *Food. Cont.*, **2018**, *92*, 183-189. DOI: 10.1016/j.foodcont.2018.05.001
- ⁵¹Pawlowska, K., Kuligowski, M., Jasinska-Kuligowska, I., Kidon, M., Aleksander Siger, A., Rudzinska, M., Nowak, J., Effect of Replacing Cocoa Powder by Carob Powder in the Muffin Sensory and Physicochemical Properties, *Plant Food. Hum. Nutr.*, **2018**, *73*, 196-202. <https://doi.org/10.1007/s11130-018-0675-0>
- ⁵²El-Naggar, E. A., Hassan, E. M., Physicochemical evaluation of carob pods (*Ceratonia siliqua* L.) powder and the effect of its addition on cupcake quality, *Arch. Agric. Sci. J.*, **2018**, *1*, 44-60. DOI:10.21608/aasj.2018.29934
- ⁵³Marrugo-Ligardo, Y. A., Severiche-Sierra, C. A., Jaimes-Morales, J., Lafont-Mendoza, J. J., Fong-Silva, W., Quality Characteristics of a Refreshing Drink Based on Carob Pulp (*Ceratonia siliqua*), *Int. J. Eng. Technol.*, **2018**, *10*, 540-544. DOI: 10.21817/ijet/2018/v10i2/181002075
- ⁵⁴Dakia, P. A., Combo, M-M., Yapo, B. M., Brou, D. K., Paquot, M., Dietary fibre content in Carob (*Ceratonia siliqua* L.) seed husk, *Int. J. Curr. Res.*, **2017**, *9*, 62190-62196. <https://www.journalcra.com/sites/default/files/issue-pdf/27577.pdf>
- ⁵⁵Berk, E., Sumnu, G., Sahin, S., Usage of carob bean flour in gluten free cakes, *Chem. Eng. Trans.*, **2017**, *57*, 1909-1914. DOI: 10.3303/CET1757319
- ⁵⁶Cervenka, L., Fruhbauerova, M., Velichova, H., Functional Properties of Muffin as Affected by Substituting Wheat Flour with Carob Powder, *Potravinarstvo Slovak J. Food Sci.*, **2019**, *13*, 212-217. <https://doi.org/10.5219/1033>
- ⁵⁷Badem, A., Alpkent, Z., Production of Ice Cream with Carob Bean Pekmez (Molasses), *Int. J. Environ. Agric. Biotechnol.*, **2018**, *3*, 28-32. <http://dx.doi.org/10.22161/ijeab/3.1.5>
- ⁵⁸Tounsi, L., Kchaou, H., Chaker, F., Bredai, S., Kechaou, N., Effect of adding carob molasses on physical and nutritional quality parameters of sesame paste, *J. Food Sci. Technol.*, **2019**, *56*, 1502-1509. <https://doi.org/10.1007/s13197-019-03640-w>
- ⁵⁹Tounsi, L., Ghazala, I., Kechaou, N. Physicochemical and phytochemical properties of Tunisian carob molasses, *J. Food Meas. Charact.*, **2020**, *14*, 20-30. <https://doi.org/10.1007/s11694-019-00263-9>
- ⁶⁰Sanli, S., Guner, O., Kilicarslan, S., Sanli, N., Screening of eighteen polyphenolic compounds in different carob pekmez by green capillary electrophoresis method, *SN Appl. Sci.*, **2020**, *2*, Article 576. <https://doi.org/10.1007/s42452-020-2387-y>
- ⁶¹Mahtout, R., Ortiz-Martinez, V. M., Salar-Garcia, M. J., Gracia, I., Hernandez-Fernandez, F. J., Rios, A. P., Zaidia, F., Sanchez-Segado, S., Lozano-Blanco, L. J., Algerian Carob Tree Products: A Comprehensive Valorization Analysis and Future Prospects, *Sustainability*, **2018**, *10*, 90-99. DOI:10.3390/su10010090
- ⁶²Papaefstathiou, E., Agapiou, A., Giannopoulos, S., Kokkinofa, R., Nutritional characterization of carobs and traditional carob products, *Food Sci. Nutr.*, **2018**, *6*, 2151-2161. DOI: 10.1002/fsn3.776

- ⁶³Benkovic, M., Bosiljkov, T., Semic, A., Jezek, D., Srecec, S., Influence of Carob Flour and Carob Bean Gum on Rheological Properties of Cocoa and Carob Pastry Fillings, *Foods*, **2019**, *8*, 66-82. DOI:10.3390/foods8020066
- ⁶⁴Fidan, H., Petkova, N., Sapundzhieva, T., Baeva, M., Goranova, Z., Slavov, A., Krastev, L., Carob Syrup and Carob Flour (*Ceratonia siliqua* L.) as Functional Ingredients in Sponge Cakes, *Carpath. J. Food Sci. Technol.*, **2019**, *11*, 71-82. <https://www.researchgate.net/publication/332427585>
- ⁶⁵Gaamouri, N., Zouhal, H., Hammami, M., Hackney, A. C., Abderrahman, A. B., Saeidi, A., El Hage, R., Ounis, O.B., Effects of polyphenol (carob) supplementation on body composition and aerobic capacity in taekwondo athletes, *Physiol. Behav.*, **2019**, *205*, 22-28. DOI: 10.1016/j.physbeh.2019.03.003
- ⁶⁶Correia, P. J., Guerreiro, J. F., Pestana, M., Martins-Loucao, M. A., Management of carob tree orchards in Mediterranean ecosystems: strategies for a carbon economy implementation, *Agroforest. Syst.*, **2017**, *91*, 295–306. DOI: 10.1007/s10457-016-9929-8
- ⁶⁷Korkmaz, N., Akin, M., Koc, A., Eyduran, S. P., Ilhan, G., Sagbas, H. I. Ercisli, S., Morphological and biochemical diversity among wild-grown carob trees (*Ceratonia siliqua* L.), *Folia Hort.*, **2020**, *32*, 1-10. DOI: 10.2478/fhort-2020-0007
- ⁶⁸Correia, P. J., Pestana, M., Exploratory Analysis of the Productivity of Carob tree (*Ceratonia siliqua*) Orchards Conducted under Dry-Farming Conditions, *Sustainability*, **2018**, *10*, 2250-2256. DOI:10.3390/su10072250
- ⁶⁹Zouari, N., Elmtili, N., Ultrasonic Influence on Carob tree (*Ceratonia siliqua* L.) rooting under in-vitro conditions, *Moroccan J. Biol.*, **2018**, *15*, 18-27. <https://www.researchgate.net/publication/331935306>
- ⁷⁰Correia, P. J., Varennes, A., Gama, F., Saavedra, T., Pestana, M., Changes in nutritional homeostasis of *Poncirus trifoliata* and *Ceratonia siliqua* as a response to different iron levels in nutrient solution, *J. Plant Nutr.*, **2018**, *41(16)*, 2103-2115. DOI:10.1080/01904167.2018.1497175
- ⁷¹Sayed, S. S., Gabr, A. M., Amin, M. A., Taha, L. S., Biochemical characterization of micropropagated *Ceratonia siliqua* L. under effect of growth regulators and light quality, *Bull. Nat. Res. Cent.*, **2020**, *44*, Article 26. DOI: 10.1186/s42269-020-0282-8
- ⁷²Jaradat, N., Zaid, A., Herbal remedies used for the treatment of infertility in males and females by traditional healers in the rural areas of the West Bank/Palestine, *BMC Complement. Alternat. Med.*, **2019**, *19*, Article 194. DOI: 10.1186/s12906-019-2617-2
- ⁷³Abarikwu, S. O., Onuah, C. L., Singh, S. K., Plants in the management of male infertility, *Andrologia*, **2020**, *52*, Article e13509. <https://doi.org/10.1111/and.13509>
- ⁷⁴O'Flaherty, C., Reactive Oxygen Species and Male Fertility, *Antioxidants*, **2020**, *9*, 287-291. DOI:10.3390/antiox9040287

Received: 17.05.2020.
Accepted: 20.06.2020.



Cu^{IV} OXIDATION STATE STABILIZATION IN THE MACROCYCLIC COMPOUND WITH PHTHALOCYANINE AND TWO FLUORO LIGANDS: DFT QUANTUM-CHEMICAL RESEARCH

Denis V. Chachkov^[a] and Oleg V. Mikhailov^{[b]*}

Keywords: Cu(IV); fluoro ligand; phthalocyanine; DFT method.

Based on the results of a quantum chemical calculation using two variants of the DFT method, and namely DFT OPBE/TZVP and DFT B3PW91/TZVP, the possibility of the existence of a copper heteroligand complex with phthalocyanine, two F⁻ ions and an oxidation state of copper (+4) which is non-traditional for this 3*d* element, have been shown. The data on the key structural parameters and also, on multiplicity of the ground state of such a complex have also been presented.

*Corresponding Authors

E-Mail: olegmkhlv@gmail.com

- [a] Kazan Department of Joint Supercomputer Center of Russian Academy of Sciences – Branch of Federal Scientific Center “Scientific Research Institute for System Analysis of the RAS”, Lobachevski Street 2/31, 420111 Kazan, Russia
[b] Kazan National Research Technological University, K. Marx Street 68, 420015 Kazan, Russia

INTRODUCTION

As has long been well known, the most typical for copper in its stable compounds is the oxidation state equal to +2 and, accordingly, oxidation state II. Compounds with a higher oxidation state of copper, namely +3, in particular tripotassium hexafluorocuprate(III) K₃[CuF₆] and heptapotassium di[hexaaxoiodato(VII)]cuprate(III) K₇[Cu(IO₆)₂], although are quite stable but uncharacteristic for the given 3*d*-element.¹ Even less characteristic for copper is the oxidation state +4, although the first of such Cu compounds, namely of dicaesium hexafluorocuprate(IV) Cs₂[CuF₆], was obtained almost 50 years ago by Harnischmacher and Hoppe.² The given metal complex was also studied in later works, in particular.³⁻⁹ Along with this fluoro-complex, compounds with a copper oxidation state of +4 that contain chemical elements with lower electronegativity, namely oxygen, for example, heteronuclear mixed oxide of lanthanum, strontium and perovskite type copper with Cu(III) and Cu(IV),^{8,9} and nitrogen, like complexes of Cu(IV) with substituted biguanides (RBig = RNHC(=NH)NHC(=NH)NH₂), namely [Cu(RBig)₂(OH)₄] and [Cu(RBig)₃]X, where R is phenyl, 4-chlorophenyl, 2-methylphenyl, X = F, Cl,^{1,10,11} are also known. After the publication of the two reviews,^{1,6} information on any new coordination compounds containing Cu(IV) did not appear in the literature. Nevertheless, there is no reason to believe that there can be no other Cu(IV) complexes.

In this connection, it seems interesting to find out whether, in principle, other copper coordination compounds in which this 3*d*-element has an oxidation state of +4, can exist under any conditions.

It has long been established that phthalocyanine (**I**) capable to stabilize a wide variety of oxidation states of *d*-elements - both low and high (see, in particular, review connection that the copper(II) complex with the such a macrocyclic ligand was accidentally obtained way back in 1927 as a by-product in the synthesis of 1,2-dicyanobenzene from 1,2-dibromobenzene in the presence of copper(I) cyanide CuCN,¹⁷) and turned out to be actually the first macrocyclic metal complex that became known to chemical science.

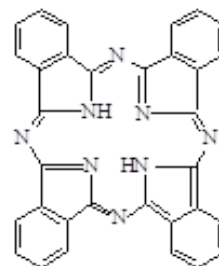


Figure 1. Structure of phthalocyanine (**I**).

Another ligand which capable of stabilizing high oxidation states, is the fluoride anion.⁴⁻⁷ In connection with this circumstance, it seems appropriate to use precisely the combination of these two ligands that takes place in the complexes having structural formula **II** to stabilize the oxidation state of Cu⁴⁺ (M is *d*-element atom, and, in particular, Cu).

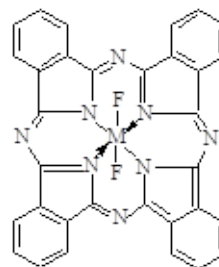


Figure 2. Proposed structure of Cu(IV) complex (**II**).

There is currently no information on such a metal complex in the literature, but nevertheless, at present, it is possible to assess the possibility of its existence using modern quantum chemical calculation methods which are now widely used for studying the structure of molecules. This is what the given investigation is devoted.

CALCULATION METHOD

Quantum-chemical calculation of the copper complex of type **II** was done by using the two versions of DFT method, namely DFT OPBE/TZVP and DFT B3PW91/TZVP. First of these methods, combining the common TZVP extended triple zeta split-valence basis set^{18,19} and the OPBE non-hybrid functional,^{20,21} as shown in the literature,^{21–25} in the case of 3*d* elements more adequately predicts the relative energy stabilities of high-spin and low-spin states, and reliably characterizes key geometric parameters of corresponding molecular structures. Second one, combining the common TZVP and B3PW91 functional,^{26,27} according to data,²⁸ has minimal value of so-called “normal error” in comparison with other variants of DFT method. Such a conclusion is in full harmony with the data of structural parameters of macrocyclic complexes of various 3*d*-elements with phthalocyanine obtained as a result of various DFT quantum-chemical calculations and in experiment.

Calculations were done by using the Gaussian09 program package.²⁹ The correspondence of the found stationary points to energy minima was proved in all cases by the calculation of second derivatives of energy with respect to atom coordinates. All equilibrium structures corresponding to minima of the potential energy surfaces had only real positive frequency values. Copper in the oxidation state +4 has 3*d*⁷ electronic configuration; in this connection, spin multiplicities 2, 4 and 6 were considered in calculation. Among the structures optimized at these multiplicities, the lowest-lying structure was selected. Parameters of molecular structures with the given multiplicities were calculated by the unrestricted methods (UOPBE and UB3PW91, respectively). The standard thermodynamic parameters of formation of this complex were calculated according to procedure described earlier.³⁰

RESULTS AND DISCUSSION

According to the data obtained by us as a result of the quantum-chemical calculation carried out using the both DFT OPBE/TZVP method and the DFT method B3PW91/TZVP, the copper complex having structural formula **II** is capable to self-existence, at least in the gas phase. Molecular structure of the given complex obtained by DFT OPBE/TZV method, is shown in Figure 3. Molecular structure obtained by the DFT B3PW91/TZVP method, looks similar. The calculated chemical bond lengths between atoms and bond angles for this macrocyclic metal complex presented in Table 1. These data show that both methods used by us, give almost identical data for all structural parameters indicated above. Some difference between the results of these methods is noted only in the case of bond lengths Cu1F1 (Cu1F2).

Table 1. Bond lengths and bond angles in the copper complex with phthalocyanine and two fluoro ligands of type **II**.

Structural parameter	Calculated by DFT	
	OPBE/TZVP	B3PW91/TZVP
Cu–N bond lengths in chelate node, pm		
Cu1N1	198.1	197.8
Cu1N2	198.1	197.8
Cu1N3	198.1	197.8
Cu1N4	198.1	197.8
Bond angles in chelate node CuN ₄ , °		
(N1Cu1N2)	90.0	90.0
(N2Cu1N3)	90.0	90.0
(N3Cu1N4)	90.0	90.0
(N4Cu1N1)	90.0	90.0
Bond angles sum, °	360.0	360.0
Non-bond angles between N atoms in N ₄ grouping, °		
(N1N2N3)	90.0	90.0
(N2N3N4)	90.0	90.0
(N3N4N1)	90.0	90.0
(N4N1N2)	90.0	90.0
Non-bond angles sum, °	360.0	360.0
Bond angles in 6-numbered ring (Cu1N2C1N8C8N3), °		
(Cu1N2C1)	125.0	125.0
(N2C1N8)	128.5	128.3
(C1N8C8)	123.0	123.4
(N8C8N3)	128.5	128.3
(C8N3Cu1)	125.0	125.0
(N3Cu1N2)	90.0	90.0
Bond angles sum ⁶ , °	720.0	720.0
Bond angles in 5-numbered ring (C2N2C1C11C12), °		
(C2N2C1)	109.8	110.0
(N2C1C11)	108.9	108.8
(C1C11C12)	106.2	106.2
(C11C12C2)	106.2	106.2
(C12C2N2)	108.9	108.8
Bond angles sum ⁵ , °	540.0	540.0
C–N bond lengths in 6-numbered chelate rings, pm		
N1C3	135.7	135.3
N1C4	135.7	135.3
N2C1	135.7	135.3
N2C2	135.7	135.3
N7C4	132.7	132.1
N7C5	132.7	132.1
C–C bond lengths in 5-numbered ring, pm		
C1C11	146.9	146.7
C11C12	140.4	139.8
C12C2	146.9	146.7
Cu–F bond length, pm		
Cu1F1 (Cu1F2)	195.1	190.7
Bond angles between fluorine, copper and nitrogen atoms, °		
F1Cu1N1 (F2Cu1N1)	90.0	90.0
F1Cu1N2 (F2Cu1N2)	90.0	90.0
F1Cu1N3 (F2Cu1N3)	90.0	90.0
F1Cu1N4 (F2Cu1N4)	90.0	90.0

As it can be seen from Figure 3, and Table 1, the complex under consideration has, on the whole, a structure of regular tetragonal bipyramid or slightly flattened octahedron (since here, the lengths of the Cu–F bonds are somewhat shorter than the lengths of the Cu–N bonds). CuN₄ chelate node of this complex has the structure of regular quadrangle (square) because the Cu–N bond lengths, distances between adjacent nitrogen atoms (N1 and N2, N2 and N3, N3 and N4, N4 and N1) absolutely identical (according to DFT OPBE/ TZVP, 198.1 and 280.1 pm and according to DFT B3PW91/TZVP, 197.8 and 279.7 pm, respectively) and all (NCuN) bond angles as well as (NNN) non-bond angles are equal to 90.0°. Copper atom is in the center of square formed by four nitrogen atoms N1, N2, N3 and N4 (Figure 3). All four 6-membered metal-chelate rings as well as all four 5-membered non-chelate rings with one nitrogen atom and four carbon atoms adjoining to 6-membered metal-chelate rings, are completely identically between themselves in the lengths of bonds between the corresponding atoms as well as in the range of bond angles in them. Both of them are strictly coplanar, because the sum of the internal bond angles in each of the 6-membered cycles (BAS⁶) is 720°, in the 5-membered ones (BAS⁵), is 540°, which coincides with the sums of the internal angles in a flat hexagon and pentagon, respectively.

This complex has a center of symmetry and therefore for it a priori one can expect that value of the electric moment of the dipole will be zero. The data for calculating this parameter (0.00 Debye units according to both DFT OPBE/TZVP and DFT B3PW91/TZVP method) are in full accordance with such an expectation.

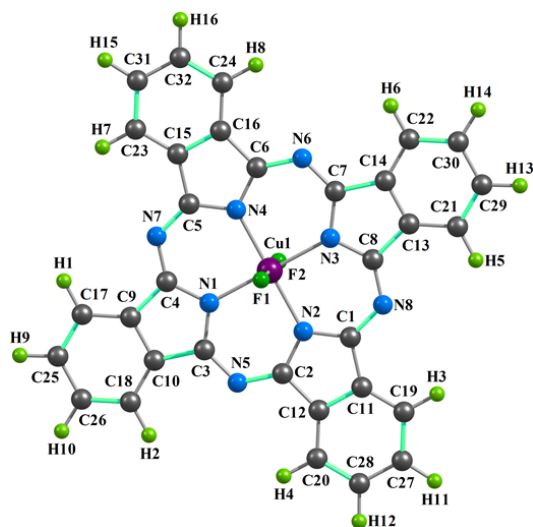


Figure 3. Molecular structure of Cu(IV) complex of type II obtained by means of DFT OPBE/TZVP quantum-chemical calculation.

The ground state of the copper complex under study, according to both calculation methods used here, is a spin doublet. It is quite expected for tetragonal-bipyramidal complexes with $3d^7$ configuration, and a coordination number of a metal ion equal to 6. Besides, according to the data of each of these methods, the nearest excited quartet state has only a little higher energy (by 1.4 kJ mol⁻¹ in the case of DFT OPBE/TZVP and 2.1 kJ mol⁻¹ in the case of DFT B3PW91/TZVP), which, apparently, makes spin-crossover in this complex a very, very likely phenomenon.

CONCLUSION

As can be seen from the data presented above, both variants of the DFT method used by us in this work, namely OPBE/TZVP and B3PW91/TZVP, quite definitely gave evidence about the possibility of the existence of copper complex [CuLF₂] containing fluoride anion (F⁻) and double deprotonated form (L²⁻) of phthalocyanine (H₂L). The copper–donor nitrogen atom and copper–fluorine interatomic distances (Table 1) in this compound correspond in their size to single bonds Cu–N and Cu–F, and, hence, the oxidation state of copper in it is namely +4. It should be noted in this connection that, according to our calculations of standard thermodynamic parameters $\Delta H_{f,298}^0$, $\Delta S_{f,298}^0$ and $\Delta G_{f,298}^0$ of the complex under study using method described in³⁰, all they are positive (339.8 kJ mol⁻¹, 1180.3 J mole⁻¹ K⁻¹ and 596.0 kJ mol⁻¹, respectively), and, hence, the given compound cannot be obtained from simple substances formed by chemical elements containing in its composition (copper, fluorine, nitrogen, carbon and hydrogen). Nevertheless, both variants of the DFT method used by us, namely OPBE/TZVP and B3PW91/TZVP, predict the possibility of the existence of this complex, and the point is now to find it in the experiment.

FUNDING INFORMATION

All quantum-chemical calculations were performed at the Kazan Department of Joint Supercomputer Center of Russian Academy of Sciences – Branch of Federal Scientific Center “Scientific Research Institute for System Analysis of the RAS”. Contribution of author Chachkov D.V. was funded by the state assignment to the Federal State Institution “Scientific Research Institute for System Analysis of the Russian Academy of Sciences” for scientific research.

CONFLICT OF INTEREST

The authors declare that they have no conflict of interest, financial or otherwise.

REFERENCES

- Popova, T. V., Aksanova, N. V. Complexes of Copper in Unstable Oxidation States. *Russ. J. Coord. Chem.*, **2003**, 29(11), 743-765. <https://doi.org/10.1023/B:RUCO.0000003432.39025.cc>
- Harnischmacher, W., Hoppe, R., Vierwertiges Kupfer: Cs₂[CuF₆]. *Angew. Chem.* **1973**, 85(13), 590-591. <https://doi.org/10.1002/ange.19730851312>
- Hoppe, R. On High Pressure Synthesis in Inorganic Solid State Fluorine Chemistry. *Israel J. Chem.* **1978**, 17(1-2), 48-52. <https://doi.org/10.1002/ijch.197800007>
- Müller, B. G. Fluoride mit Kupfer, Silber, Gold und Palladium. *Angew. Chem.* **1987**, 99(11), 1120-1135. <https://doi.org/10.1002/ange.19870991105>
- Hoppe, R. Neues über Metalle mit Sauerstoff oder Fluor als Liganden. *Angew. Chem.*, **1981**, 93(1), 64-88. <https://doi.org/10.1002/ange.19810930108>

- ⁶Kiselev, Yu. M., Tretiyakov, Yu. D., The problem of oxidation state stabilisation and some regularities of a Periodic system of the elements. *Russ. Chem. Revs.*, **1999**, 68(5), 365-379. <https://doi.org/10.1070/RC1999v068n05ABEH000496>
- ⁷Grannec, J., Some physical properties of d-transition metal fluorides in unusual oxidation states. *J. Fluorine Chem.* **1984**, 25(1), 83-90. [https://doi.org/10.1016/S0022-1139\(00\)81198-7](https://doi.org/10.1016/S0022-1139(00)81198-7)
- ⁸Demazeau, G., Darracq, S., Choy, J. H., High oxygen pressures and the stabilization of a new mixed valence Cu(III)/Cu(IV). *High Pressure Res.*, **1994**, 12(4-6), 323-328. <https://doi.org/10.1080/08957959408201677>
- ⁹Darracq, S., Kang, S. G., Choy, J. H., Demazeau, G., Stabilization of the Mixed Valence Cu(III)/Cu(IV) in the Perovskite Lattice of La_{1-x}Sr_xCuO₃ under High Oxygen Pressure. *J. Solid State Chem.*, **1995**, 114(1), 88-94. <https://doi.org/10.1006/jssc.1995.1013>
- ¹⁰Bicher, M., Jinga, D., *Rom. Biotechnol. Lett.*, **1999**, 4(2), 129-140. (cited by [1])
- ¹¹Bicher, M., Oprea, O., *Rom. Biotechnol. Lett.* **1999**, 4(2), 151-158. (cited by [1])
- ¹²Mamardashvili, G. M., Mamardashvili, N. Z., Koifman, O. I., Self-assembling systems based on porphyrins. *Russ. Chem. Revs.*, **2008**, 77(1), 59-75. <https://doi.org/10.1070/RC2008v077n01ABEH003743>
- ¹³Sliva, W., Mianovska, B., Metalloporphyrin arrays. *Transit. Met. Chem.*, **2000**, 25(5), 491-504. <https://doi.org/10.1023/A:1007054025169>
- ¹⁴Chelevina, O. G., Malyasova, A. S., 40 years with porphyrazines. *J. Porph. Phthalocyanines*, **2019**, 23(11), 1261-1264. <https://doi.org/10.1142/S1088424619300246>
- ¹⁵Thomas, A. L., *Phthalocyanines*. Research & Applications, CRC Press, **1990**.
- ¹⁶Lomova, T. N., *Axial coordinated metal porphyrins in science and practice*. Moscow, URSS, **2018**.
- ¹⁷De Diesbach, H., von der Weid, E., Quelques sels complexes des o-dinitriles avec le cuivre et la pyridine. *Helv. Chim. Acta*, **1927**, 10(1), 886-888. <https://doi.org/10.1002/hlca.192701001110>
- ¹⁸Schaefer, A., Horn, H., Ahlrichs, R., Fully optimized contracted Gaussian basis sets for atoms Li to Kr. *J. Chem. Phys.* **1992**, 97(4), 2571-2577. <https://doi.org/10.1063/1.463096>
- ¹⁹Schaefer, A., Huber, C., Ahlrichs, R., Fully optimized contracted Gaussian basis sets of triple zeta valence quality for atoms Li to Kr. *J. Chem. Phys.*, **1994**, 100(8), 5829-5835. <https://doi.org/10.1063/1.467146>
- ²⁰Hoe, W. M., Cohen, A., Handy, N. C., Assessment of a new local exchange functional OPTX. *Chem. Phys. Lett.*, **2001**, 341(3-4), 319-328. [https://doi.org/10.1016/S0009-2614\(01\)00581-4](https://doi.org/10.1016/S0009-2614(01)00581-4)
- ²¹Perdew, J. P., Burke, K., Ernzerhof, M., Generalized Gradient Approximation Made Simple. *Phys. Rev. Lett.*, **1997**, 78 (7), 1396-1396. <https://doi.org/10.1103/PhysRevLett.78.1396>
- ²²Paulsen, H., Duelund, L., Winkler, H., Toftlund, H., Trautwein, A. X., Free Energy of Spin-Crossover Complexes Calculated with Density Functional Methods. *Inorg. Chem.*, **2001**, 40(9), 2201-2203. <https://doi.org/10.1021/ic000954q>
- ²³Swart, M., Groenhof, A. R., Ehlers, A. W., Lammertsma, K., Validation of Exchange-Correlation Functionals for Spin States of Iron Complexes. *J. Phys. Chem. A*, **2004**, 108(25), 5479-5483. <https://doi.org/10.1021/jp049043i>
- ²⁴Swart, M., Ehlers, A. W., Lammertsma, K., Performance of the OPBE exchange-correlation functional. *Mol. Phys.* **2004**, 102(23), 2467-2474. <https://doi.org/10.1080/0026897042000275017>
- ²⁵Swart, M., Metal-ligand bonding in metallocenes: Differentiation between spin state, electrostatic and covalent bonding. *Inorg. Chim. Acta*, **2007**, 360(1), 179-189. <https://doi.org/10.1016/j.ica.2006.07.073>
- ²⁶Becke, A. D., Density-functional exchange-energy approximation with correct asymptotic behavior. *Phys. Revs. A*, **1988**, 38(6), 3098-3100. <https://doi.org/10.1103/PhysRevA.38.3098>
- ²⁷Perdew, J. P., Burke, K., Wang, Y. Generalized gradient approximation for the exchange-correlation hole of a many-electron system. *Phys. Revs. B*, **1996**, 54(23), 16533-16539. <https://doi.org/10.1103/PhysRevB.54.16533>
- ²⁸Medvedev, M. G., Bushmarinov, I. S., Sun, J., Perdew, J. P., Lyssenko, K. A., Density functional theory is straying from the path toward the exact functional. *Science*, **2017**, 355(6320), 49-52. <https://doi.org/10.1126/science.aah5975>
- ²⁹Gaussian 09, Revision A.01, Frisch M.J, Trucks G.W., Schlegel H.B., Scuseria G.E., Robb M.A., Cheeseman J.R., Scalmani G., Barone V., Mennucci B., Petersson G.A., Nakatsuji H., Caricato M., Li H., Hratchian H.P., Izmaylov A.F., Bloino J., Zheng G., Sonnenberg J.L., Hada M., Ehara M., Toyota K., Fukuda R., Hasegawa J., Ishida M., Nakajima T., Honda Y., Kitao O., Nakai H., Vreven T., Montgomery J.A., Jr., Peralta J.E., Ogliaro F., Bearpark M., Heyd J.J., Brothers E., Kudin K.N., Staroverov V.N., Kobayashi R., Normand J., Raghavachari K., Rendell A., Burant J.C., Iyengar S.S., Tomasi J., Cossi M., Rega N., Millam J.M., Klene M., Knox J.E., Cross J.B., Bakken V., Adamo C., Jaramillo J., Gomperts R., Stratmann R.E., Yazyev O., Austin A.J., Cammi R., Pomelli C., Ochterski J.W., Martin R.L., Morokuma K., Zakrzewski V.G., Voth G.A., Salvador P., Dannenberg J.J., Dapprich S., Daniels A.D., Farkas O., Foresman J.B., Ortiz J.V., Cioslowski J., and Fox D.J., Gaussian, Inc., Wallingford CT, **2009**.
- ³⁰Ochterski, J. W., *Thermochemistry in Gaussian*. Gaussian, Inc., Wallingford CT, **2000**.

Received: 03.06.2020.

Accepted: 22.06.2020.